Article
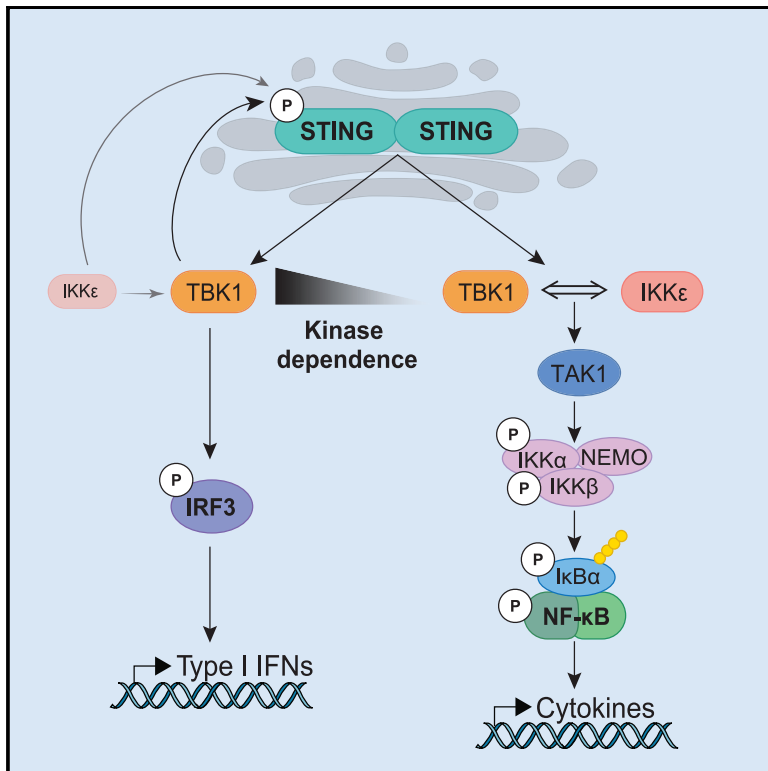
TBK1 and IKKε Act Redundantly to Mediate STING-Induced NF-κB Responses in Myeloid Cells

Graphical Abstract

Authors

Katherine R. Balka, Cynthia Louis, Tahnee L. Saunders, ..., Benjamin T. Kile, Seth L. Masters, Dominic De Nardo

Correspondence

dominic.denardo@monash.edu

In Brief

Activation of NF-κB via STING is considered to be exclusively dependent on TBK1. Balka et al. now show that, although TBK1 and its kinase activity are critical for IRF3 activation and type I IFNs, it is dispensable for NF-κB. Instead, TBK1 and IKKε act redundantly to mediate STING-induced NF-κB responses.

Highlights

- TBK1 is dispensable for NF-κB activation downstream of STING *in vitro* and *in vivo*

- TBK1 and IKKε act redundantly to elicit STING-induced NF-κB activation

- STING-NF-κB is less sensitive to TBK1/IKKε kinase inhibition than type I IFN

- TAK1 and IKK complexes are required for STING-mediated NF-κB responses

CellPress

TBK1 and IKKε Act Redundantly to Mediate STING-Induced NF-κB Responses in Myeloid Cells

Katherine R. Balka,[1,4,5] Cynthia Louis,[1,4] Tahnee L. Saunders,[5] Amber M. Smith,[8] Dale J. Calleja,[1,4] Damian B. D'Silva,[1,4] Fiona Moghaddas,[1,4] Maximilien Tailler,[5] Kate E. Lawlor,[6] Yifan Zhan,[2,4] Christopher J. Burns,[3,4] Ian P. Wicks,[1,4,9] Jonathan J. Miner,[8] Benjamin T. Kile,[5,7,10] Seth L. Masters,[1,4,10] and Dominic De Nardo[1,4,5,10,11,*]

[1]Inflammation Division, The Walter and Eliza Hall Institute of Medical Research, 1G Royal Parade, Parkville, VIC 3052, Australia
[2]Immunology Division, The Walter and Eliza Hall Institute of Medical Research, 1G Royal Parade, Parkville, VIC 3052, Australia
[3]Chemical Biology Division, The Walter and Eliza Hall Institute of Medical Research, 1G Royal Parade, Parkville, VIC 3052, Australia
[4]Department of Medical Biology, The University of Melbourne, Parkville, VIC 3010, Australia
[5]Department of Anatomy and Developmental Biology, Monash Biomedicine Discovery Institute, Monash University, Clayton, VIC 3800, Australia
[6]Centre for Innate Immunity and Infectious Diseases, Hudson Institute of Medical Research, Department of Molecular and Translational Science, Monash University, Clayton, VIC 3168, Australia
[7]Health and Medical Sciences Faculty Office, University of Adelaide, Adelaide, SA 5005, Australia
[8]Departments of Medicine, Molecular Microbiology, and Pathology and Immunology, Washington University School of Medicine, St. Louis, MO, USA
[9]Rheumatology Unit, Royal Melbourne Hospital, Parkville, VIC 3050, Australia
[10]Senior author
[11]Lead Contact
*Correspondence: dominic.denardo@monash.edu
https://doi.org/10.1016/j.celrep.2020.03.056

SUMMARY

Stimulator of Interferon Genes (STING) is a critical component of host innate immune defense but can contribute to chronic autoimmune or autoinflammatory disease. Once activated, the cyclic guanosine monophosphate (GMP)-adenosine monophosphate (AMP) (cGAMP) synthase (cGAS)-STING pathway induces both type I interferon (IFN) expression and nuclear factor-κB (NF-κB)-mediated cytokine production. Currently, these two signaling arms are thought to be mediated by a single upstream kinase, TANK-binding kinase 1 (TBK1). Here, using genetic and pharmacological approaches, we show that TBK1 alone is dispensable for STING-induced NF-κB responses in human and mouse immune cells, as well as *in vivo*. We further demonstrate that TBK1 acts redundantly with IκB kinase ε (IKKε) to drive NF-κB upon STING activation. Interestingly, we show that activation of IFN regulatory factor 3 (IRF3) is highly dependent on TBK1 kinase activity, whereas NF-κB is significantly less sensitive to TBK1/IKKε kinase inhibition. Our work redefines signaling events downstream of cGAS-STING. Our findings further suggest that cGAS-STING will need to be targeted directly to effectively ameliorate the inflammation underpinning disorders associated with STING hyperactivity.

INTRODUCTION

The innate immune system induces a rapid response following the recognition of pathogens or endogenous danger signals by stimulating the release of inflammatory mediators. This response is facilitated by families of highly conserved pattern recognition receptors (PRRs) that are expressed by innate immune cells, such as macrophages and dendritic cells (De Nardo, 2017). Once activated, many PRRs initiate downstream signaling cascades, leading to the secretion of cytokines, chemokines, and interferons (IFNs), producing a local inflammatory milieu, the recruitment of additional immune cells, and ultimately the resolution of the insult and initiation of tissue repair. Nucleic acid sensing PRRs are particularly important for initiating an anti-viral immune response following infection. There are two major cytosolic sensors for double-stranded DNA (dsDNA): the inflammasome-forming protein absent in melanoma-2 (AIM2), which induces maturation of the cytokines interleukin-1β (IL-1β) and IL-18 and an inflammatory form of cell death known as pyroptosis (Latz et al., 2013); and cyclic guanosine monophosphate (GMP)-adenosine monophosphate (AMP) (cGAMP) synthase (cGAS), which is important for inducing a potent type I IFN response to viral infection. cGAS is unique among PRRs due to its enzymatic activity as a nucleotidyl transferase that cyclizes ATP and GTP by phosphodiester bonds, resulting in the formation of the endogenous cyclic dinucleotide (CDN) 2′3′-cGAMP (Ablasser et al., 2013; Diner et al., 2013; Sun et al., 2013; Zhang et al., 2013). 2′3′-cGAMP then acts as a specific second messenger to activate the endoplasmic reticulum (ER)-resident protein Stimulator of Interferon Genes (STING). Although 2′3′-cGAMP is the only known mammalian CDN, similar CDNs (e.g., 3′3′-cGAMP, cyclic-di-AMP, cyclic-di-GMP) are released from bacteria during infection that can also bind directly to STING and induce its activation (Burdette et al., 2011; McWhirter et al., 2009; Woodward et al., 2010). The absolute requirement of STING for mediating an anti-viral immune response against DNA viruses, such as herpes simplex virus-1 (HSV-1), has been demonstrated through the use of cGAS- and STING-deficient mice (Ishikawa et al., 2009; Li et al., 2013). On the other hand,

the induction of type I IFNs by STING can have unfavorable effects in the context of bacterial infection (e.g., *Listeria monocytogenes*) by promoting bacterial growth and survival (Marinho et al., 2017).

The inability of cGAS to precisely discriminate the origin and length of dsDNA that it encounters also enables sensing of mislocalized host-derived dsDNA in the cytosol, such as genomic or mitochondrial DNA (Rongvaux et al., 2014; West et al., 2015; White et al., 2014). Hence the cGAS-STING pathway is pathogenic in primary immune disorders associated with an accumulation of cytosolic self-DNA, including Aicardi-Goutières syndrome and certain forms of lupus (Ablasser et al., 2014; Ahn et al., 2012; Gall et al., 2012; Gkirtzimanaki et al., 2018). Recent work has suggested that failure to induce mitophagy (the process of removing damaged mitochondria) leads to excessive circulating mtDNA that can elicit aberrant inflammation via cGAS-STING and contribute to aging-related neurodegenerative conditions, such as Parkinson's disease (Sliter et al., 2018). Perhaps the clearest demonstration of the importance of controlling STING signaling was the identification of a life-threatening autoinflammatory condition, termed STING-associated vasculopathy with onset in infancy (SAVI) (Liu et al., 2014). The chronic inflammation observed in SAVI patients was found to be driven by *de novo* autoactivating mutations in *TMEM173* (the gene encoding STING), leading to constitutive STING activation that manifests early in life as inflammatory skin lesions, small-vessel vasculitis, and in some cases, severe pulmonary complications (Clarke et al., 2016; Liu et al., 2014).

To date, the majority of studies examining cGAS-STING have focused primarily on the potent type I IFN response; however, STING also triggers a prominent pro-inflammatory cytokine response (e.g., tumor necrosis factor [TNF], IL-1β, and IL-6) through the activity of NF-κB (Ishikawa and Barber, 2008; Ishikawa et al., 2009). CDN binding induces significant conformational changes in preformed STING dimers, initiating translocation from the ER to Golgi compartments and the recruitment of the serine-threonine protein kinase, TANK-binding kinase 1 (TBK1). TBK1 subsequently phosphorylates residues in the C-terminal tail (CTT) region of STING, allowing the recruitment of IFN regulatory factor 3 (IRF3) molecules and their subsequent phosphorylation by TBK1 (Liu et al., 2015; Tanaka and Chen, 2012). Activated IRF3 dimers then translocate to the nucleus and induce the expression and secretion of type I IFNs (e.g., IFNβ), which in turn leads to the production of numerous IFN-stimulated genes (ISGs), inducing a robust anti-viral state. In addition, NF-κB, along with other transcription factors, synergizes with IRF3 by collectively binding a specific enhancer region within the IFNβ promoter, termed the enhanceosome, resulting in maximal IFNβ expression (Smale, 2010). Currently, it is widely accepted that in addition to eliciting the type I IFN response, TBK1 is also responsible for inducing NF-κB activation downstream of STING, as demonstrated in TBK1-deficient and TBK1 RNAi-silenced mouse embryonic fibroblasts (MEFs) (Abe and Barber, 2014).

Both TBK1 and its homolog, IκB kinase (IKK) ε (IKKε, also known as IKKi), were initially found to induce NF-κB luciferase reporter activity in overexpression studies (Shimada et al., 1999;

Tojima et al., 2000). However, experiments using *Tbk1*$^{-/-}$, *IKKε*$^{-/-}$, and *Tbk1*$^{-/-}$/*IKKε*$^{-/-}$ mice or TBK1/IKKε chemical inhibition have demonstrated that although TBK1, and to a much lesser extent IKKε, have an essential role in IRF3-mediated IFNβ production, they are not required for NF-κB activation in response to Toll-like receptors (TLRs), IL-1β, or TNF (Clark et al., 2009; Hemmi et al., 2004; Perry et al., 2004). Several additional lines of evidence suggest that STING may induce NF-κB activity via a TBK1-independent mechanism. First, the cGAS-STING pathway predates the evolutionary emergence of IFNs, suggesting it may have originally evolved as an activator of NF-κB signaling. Second, despite the highly conserved nature of STING across phyla, the presence of the CTT region, critical to IFN induction, is observed only in vertebrates (Margolis et al., 2017). Therefore, although physiological *Drosophila melanogaster* and *Nematostella vectensis* STING can induce only pathways homologous to NF-κB, the addition of the CTT of human STING to either species confers the ability to trigger type I IFN activity (Kranzusch et al., 2015; Martin et al., 2018). Several studies have further shown that removal of a part or the entire CTT of human STING ablates IFN activity, but not that of NF-κB (Cerboni et al., 2017; Chen et al., 2014). Third, STING is known to be heavily modified posttranslationally, including via phosphorylation, palmitoylation, ubiquitination, and SUMOylation (Baker et al., 2017). Although certain STING modifications, such as palmitoylation, have been shown to be critical for both type I IFN and NF-κB responses (Haag et al., 2018), ubiquitination of STING at lysine (K) residues 244 and 288 is specifically required for trafficking of STING from the ER to the Golgi, where it elicits type I IFN production (Ni et al., 2017; Stempel et al., 2019). In contrast, STING-mediated NF-κB responses appear to be independent of K244 and K288 ubiquitination, demonstrating that these responses may occur prior to Golgi relocalization, suggesting that spatial uncoupling of type I IFN and NF-κB signaling can occur (Ni et al., 2017; Stempel et al., 2019). Furthermore, Konno et al. (2013) found that phosphorylation of STING at serine residues 358 and 366, although critical for IRF3 activation, was unnecessary for NF-κB activity. Finally, Dunphy et al. (2018) demonstrated that DNA damage induced by the chemotherapeutic agent etoposide elicits non-canonical STING activation that primarily promotes NF-κB in a TBK1-independent manner, rather than an IRF3 response. These observations raise the critical question of whether TBK1 alone directs STING-mediated NF-κB responses.

Here, utilizing both genetic deletion and pharmacological inhibition of TBK1 in murine and human innate immune cells, we demonstrate that although TBK1 and its kinase activity are critical for the phosphorylation of IRF3 and subsequent production of IFNβ in response to STING activation, NF-κB activity and pro-inflammatory cytokine production can occur in a manner independent of TBK1. We further show that STING-NF-κB responses are actually mediated via a TBK1/IKKε redundant mechanism. Based on these observations, we present a revised model of STING signaling events leading to type I IFN and NF-κB responses. Our findings shed light on the molecular mechanisms of cGAS-STING signaling and have important implications for the effective therapeutic targeting of cGAS-STING-related diseases.

RESULTS

Primary Macrophages Deficient in TBK1 Exhibit Normal STING-NF-κB Responses

TBK1 is thought to be essential for STING-induced NF-κB activation; however, this has been formally shown only in MEFs (Abe and Barber, 2014). Hence we first assessed STING responses in primary macrophages and mice deficient in TBK1. Deletion of TBK1 induces embryonic lethality in mice (Bonnard et al., 2000; Lafont et al., 2018; Xu et al., 2018); we therefore utilized mice carrying floxed alleles of *Tbk1* (*Tbk1$^{fl/fl}$*) and crossed these to ROSA26-CreERT2 (*RosaCre*) animals, allowing for inducible ubiquitous *in vivo* deletion of *Tbk1* upon treatment with tamoxifen. We generated primary bone marrow-derived macrophages (BMDMs) from tamoxifen-treated *Tbk1$^{fl/fl}$* (wild-type [WT]) and *Tbk1$^{fl/fl}$* × *RosaCre* (TBK1 knockout [KO]) mice, observing significant depletion in levels of TBK1 protein expression, albeit variable in cells from individual TBK1 KO animals (Figures 1A and S1). Of note, TBK1-deficient primary BMDMs treated with DMXAA or 2′3′-cGAMP exhibited reduced phosphorylation of IRF3 (p-IRF3) and STING (p-STING) compared with their WT counterparts, whereas the activation of NF-κB p65 (p-p65) and IκBα degradation remained normal (Figures 1A and S1). We next treated primary WT and TBK1 KO BMDMs with several activators of STING (DMXAA, 2′3′-cGAMP) or cGAS-STING (DNA isolated from herring testes [HT-DNA], HSV-1) and directly compared their ability to produce IFNβ and TNF protein. Significant reductions in IFNβ secretion in response to STING activation were clear from TBK1-deficient BMDMs in response to all stimuli (Figure 1B), whereas TNF levels were similar to those produced from WT cells in response to direct STING activation with DMXAA and cGAMP (Figure 1C). Interestingly, TBK1-deficient BMDMs did show a consistent reduction in TNF in response to HT-DNA and HSV-1, albeit not to statistically significant levels (Figure 1C). These data demonstrate that NF-κB responses are maintained in TBK1-deficient macrophages upon STING activation, whereas in contrast, IRF3 activity and IFNβ secretion are significantly reduced.

### TBK1-Deficient Mice Maintain NF-κB Responses following DMXAA Challenge

To determine whether TBK1 is required for STING-NF-κB signaling *in vivo*, we pre-treated *Tbk1$^{fl/fl}$* (WT) and *Tbk1$^{fl/fl}$* × *RosaCre* (TBK1 KO) mice for 4 days with tamoxifen to induce *Tbk1* gene deletion before acute challenge with DMXAA or a vehicle control (Ctrl). Intraperitoneal injection of DMXAA led to increased expression of type I IFNs and inflammatory cytokine genes measured from WT spleens. TBK1 deficiency significantly reduced expression of *Ifna1*, *Ifna4*, and *Isg15*, with a similar trend in *Ifnb1* (Figures 2A–2D). In contrast, the expression levels of the NF-κB-dependent genes, *Il1b*, *Il6*, and *Ccl4*, were not reduced (Figures 2E–2H). Of note, *Tnf* expression levels from mice deficient in TBK1 appeared to decrease, albeit not significantly (Figure 2H). This is in line with recent findings demonstrating that in response to STING activation, a conventional dendritic cells subset (cDC2) elicits TNF production in an NF-κB-independent but TBK1-dependent manner *in vivo* (Mansouri et al., 2019).

Thus, the expression of TNF may not be a clear readout of STING-mediated NF-κB activity *in vivo*. Consistent with our findings *in vitro*, these data show that *in vivo*, the induction of NF-κB-dependent responses downstream of STING activation can occur independently of TBK1.

TBK1 Is Dispensable for NF-κB Activation Downstream of STING

As we noted above, BMDMs generated from *Tbk1$^{fl/fl}$* × *Rosa-Cre$^+$* mice treated with tamoxifen retained a small amount of detectable TBK1 protein (Figures 1A and S1A). We therefore used CRISPR/Cas9 gene editing to generate TBK1-deficient immortalized BMDMs (iBMDMs) by targeting exon 4 of the *Tbk1* gene locus with doxycycline-inducible single guide RNAs (sgRNAs) (Figure S2A). To ensure our results were not affected by residual TBK1 levels in the pool of CRISPR-targeted cells, we generated single-cell clones deficient for TBK1 from the polyclonal population. We hypothesized that if TBK1 is required for both IRF3 and NF-κB activation, macrophages lacking TBK1 would phenocopy *Sting$^{−/−}$* cells. We examined STING signaling in response to DMXAA or 2′3′-cGAMP stimulation in WT, TBK1^{KO}, and *Sting$^{−/−}$* iBMDMs by immunoblotting. As expected, TBK1 deletion prevented phosphorylation of IRF3 (Figures 3A and 3B). Consistent with previous reports, phosphorylation of STING at S365 (S366 in humans) was also significantly reduced in cells lacking TBK1 (Liu et al., 2015), but not ablated (Figures 3A and 3B). In comparison, NF-κB p65 activation was relatively normal, albeit with slightly delayed kinetics, following STING activation in TBK1^{KO} iBMDMs (Figures 3A and 3B). Not surprisingly, activation of both IRF3 and NF-κB was absent in *Sting$^{−/−}$* iBMDMs. We observed consistent results from human TBK1^{KO} THP-1 monocytic cells following activation of STING with the modified CDN, 2′3′-cyclic di-AMP (CDA) (PS)2 (RR), which also retained p-p65 despite TBK1 deficiency (Figure S2B). We further activated STING in WT, TBK1^{KO}, and *Sting$^{−/−}$* iBMDMs, and examined cytokine secretion, observing a complete loss of IFNβ production in the absence of TBK1 or STING (Figure 3C). In stark contrast, secretion of TNF was normal in the TBK1^{KO} cells, whereas *Sting$^{−/−}$* iBMDMs remained unresponsive (Figure 3D). These results were consistent when we compared cytokine responses across several TBK1-deficient iBMDM populations we generated via CRISPR (Figures S2C and S2D). Furthermore, the kinetics of NF-κB-dependent cytokines, TNF, IL-1β, and IL-12p40, appeared similar up to 8 h after STING activation between WT and TBK1-deficient macrophages (Figures S2E–S2J). These data clearly demonstrate that STING-mediated NF-κB signaling and cytokine responses are not lost in the absence of TBK1 expression.

To assess STING activation in a disease-relevant, ligand-free system, we next developed an *in vitro* model of the autoinflammatory disease SAVI that is caused by autoactivating mutations in the gene encoding human STING, *TMEM173* (Liu et al., 2014). We modeled a form of SAVI caused by an arginine-to-serine substitution at position 284 (R284S) of STING that we and others recently described (Konno et al., 2018; Saldanha et al., 2018). We used a doxycycline-inducible lentiviral system allowing controlled expression of WT STING, STING R284S, or an empty vector (EV) Ctrl on WT and TBK1-deficient genetic

A
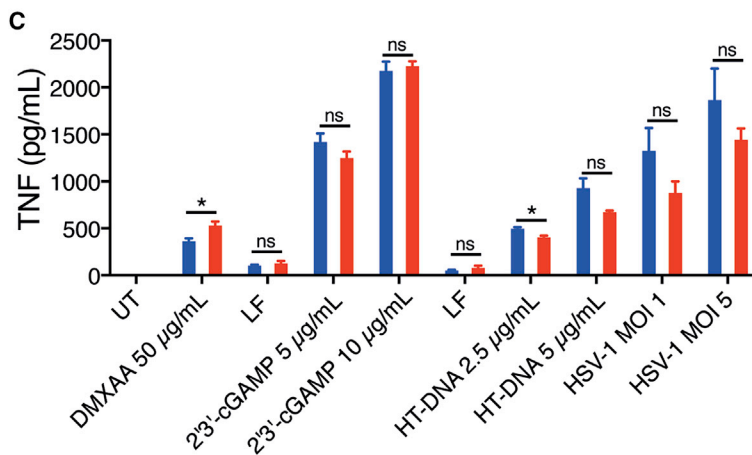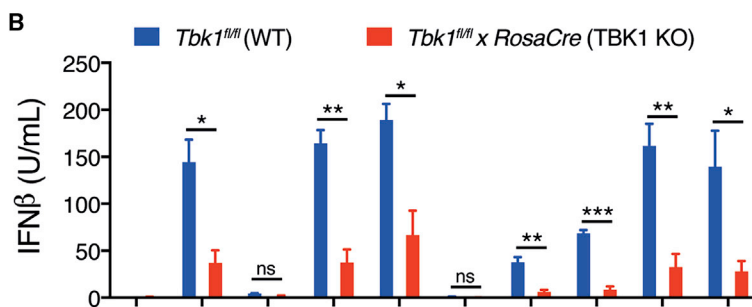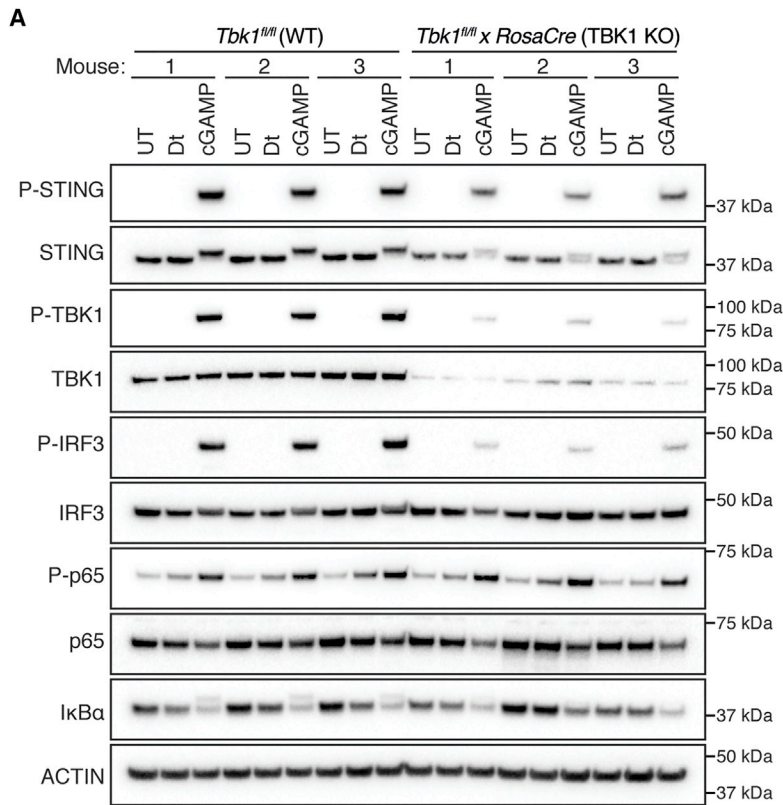
Figure 1. Primary TBK1-Deficient BMDMs Have Normal STING-NF-κB Responses

(A) Primary BMDMs from tamoxifen-treated *Tbk1*$^{fl/fl}$ (WT) and *Tbk1*$^{fl/fl}$ × *RosaCre* (TBK1 KO) mice were left untreated (UT) or stimulated with 10 μg/mL 2'3'-cGAMP in digitonin reagent (Dt) or Dt alone for 2 h, before cells were lysed for immunoblotting with the indicated antibodies. Data from three mice of each genotype are shown as representative of two independent experiments.

(B and C) Primary BMDMs from tamoxifen-treated *Tbk1*$^{fl/fl}$ (WT) and *Tbk1*$^{fl/fl}$ × *RosaCre* (TBK1 KO) mice left untreated (UT) or stimulated as indicated for 6 h before cell supernatants were collected to measure levels of secreted IFNβ (B) and TNF (C) by ELISA. Data represent the mean from three combined experiments + SEM. *p < 0.05, **p < 0.01, ***p < 0.001, not significant (ns) comparing *Tbk1*$^{fl/fl}$ (WT) versus *Tbk1*$^{fl/fl}$ × *RosaCre* (TBK1 KO) BMDMs as determined by unpaired Student's t test.

See also Figure S1.

B

C
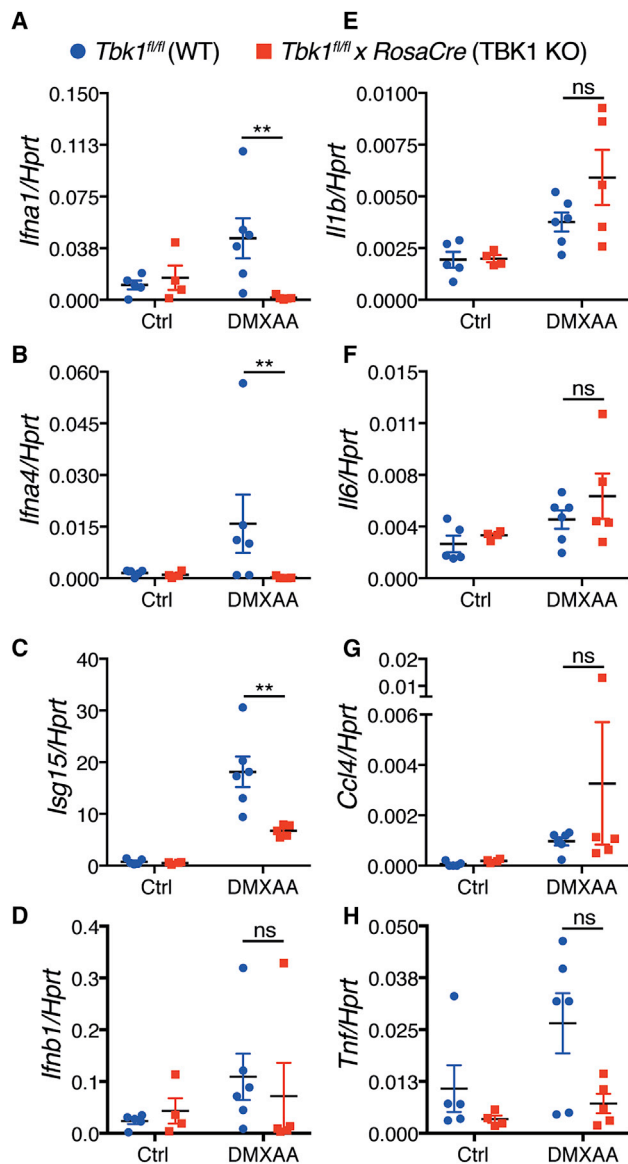
Figure 2. TBK1-Deficient Mice Challenged with DMXAA Have No Defects in NF-κB-Mediated Cytokine Expression

(A–H) Tamoxifen-treated *Tbk1 fl/fl* (WT) and *Tbk1 fl/fl × RosaCre* (TBK1 KO) mice received intraperitoneal injection of either a DMSO control (Ctrl) or 500 µg (~20 mg/kg) DMXAA for 2 h. Mice were sacrificed before RNA was isolated from splenic tissue, and type I IFN genes, *Ifna1* (A), *Ifna4* (B), *Isg15* (C), and *Ifnb1* (D), and NF-κB-dependent cytokine genes, *Il1b* (E), *Il6* (F), *Ccl4* (G), and *Tnf* (H), were measured by qPCR. Data represent the mean combined for 4–6 mice per group ± SEM. **p < 0.01, not significant (ns) comparing *Tbk1 fl/fl* (WT) versus *Tbk1 fl/fl × RosaCre* (TBK1 KO) mice in the DMXAA-treated groups as determined by Mann-Whitney test.

backgrounds. Overexpression of WT STING did not lead to autoactivation of downstream signaling in either WT or TBK1[KO] iBMDMs (Figure 3E). On the other hand, expression of STING R284S induced a strong signaling response in WT iBMDMs, whereas iBMDMs lacking TBK1 showed negligible p-IRF3 but maintained normal activation of NF-κB p65 (Figure 3E). In line

with these findings, IFNβ, but not TNF secretion, was ablated in the absence of TBK1 after STING R284S induction by doxycycline (Figures 3F and 3G). These data further indicate that TBK1 is expendable for NF-κB responses downstream of STING activation.

TBK1 and IKKε Act Redundantly to Elicit STING-Induced NF-κB Activation

Having demonstrated that TBK1 is dispensable for NF-κB activation downstream of STING, we wanted to examine a possible role for the TBK1 homolog, IKKε, in this response. To this end, we further generated IKKε[KO] and TBK1[KO]/IKKε[KO] iBMDMs using CRISPR/Cas9 and tested their ability to elicit signaling in response to STING activation. Consistent with our previous data, while p-IRF3 was lost and p-STING was significantly reduced in TBK1[KO] cells, NF-κB p-p65 was maintained with slightly delayed kinetics (Figure 4A). In contrast with TBK1[KO] macrophages, IKKε[KO] iBMDMs showed only minor impairment in their ability to induce phosphorylation of both IRF3 and STING (Figure 4A). Similar to loss of TBK1, cells lacking IKKε retained relatively normal phosphorylation of NF-κB p65, albeit slightly reduced at later time points, following STING activation (Figure 4A). Most notably, however, TBK1[KO]/IKKε[KO] iBMDMs were completely unresponsive upon STING activation, showing no detectable phosphorylation of STING and IRF3, and only basal levels of NF-κB p65 activity (Figure 4A). In line with our signaling data, TBK1[KO] and TBK1[KO]/IKKε[KO] iBMDMs were unable to produce IFNβ, whereas WT and IKKε[KO] macrophages secreted similar amounts in response to both DMXAA and 2′3′-cGAMP (Figures 4C and 4E). Meanwhile, production of TNF was normal in TBK1[KO] and IKKε[KO] iBMDMs (Figures 4D and 4F). Significantly, macrophages lacking both TBK1 and IKKε were unable to secrete TNF in response to STING activation (Figures 4D and 4F). Consistent with previous reports (Hemmi et al., 2004; Perry et al., 2004), we found that loss of TBK1, IKKε, or both TBK1 and IKKε had no effect on lipopolysaccharide (LPS)-induced activation of NF-κB p65 or subsequent TNF production (Figures 4B and 4D). Together, these data demonstrate that TBK1 and IKKε can act redundantly in order to activate STING-NF-κB responses, a mechanism that is distinct from their role in TLR4 signaling.

STING-Induced NF-κB Responses Are Less Sensitive to TBK1 and IKKε Kinase Inhibition Than Type I IFNs

Having established that TBK1 and IKKε act redundantly to drive STING-NF-κB, we next assessed the effects of inhibiting their kinase activity on STING responses. To do this, we pre-treated primary BMDMs with the semi-selective TBK1/IKKε kinase inhibitors, WEHI-112 (Louis et al., 2019) or MRT67307, using DMSO as a vehicle Ctrl, 1 h prior to STING activation. As previously reported, we observed paradoxical autophosphorylation of TBK1 in the presence of WEHI-112 and MRT67307 (Louis et al., 2019), but a loss of DMXAA-induced p-IRF3 (Figure S3A). Interestingly, in the presence of TBK1/IKKε kinase inhibition, we still observed increased p-p65 levels, although reduced relative to Ctrl-treated BMDMs (Figure S3A). Similar results were seen from BMDMs activated with the TLR3 ligand polyinosinic:polycytidylic acid (polyI:C) following WEHI-112 or MRT67307 pre-treatment (Figure S3A). We next examined STING-induced signaling
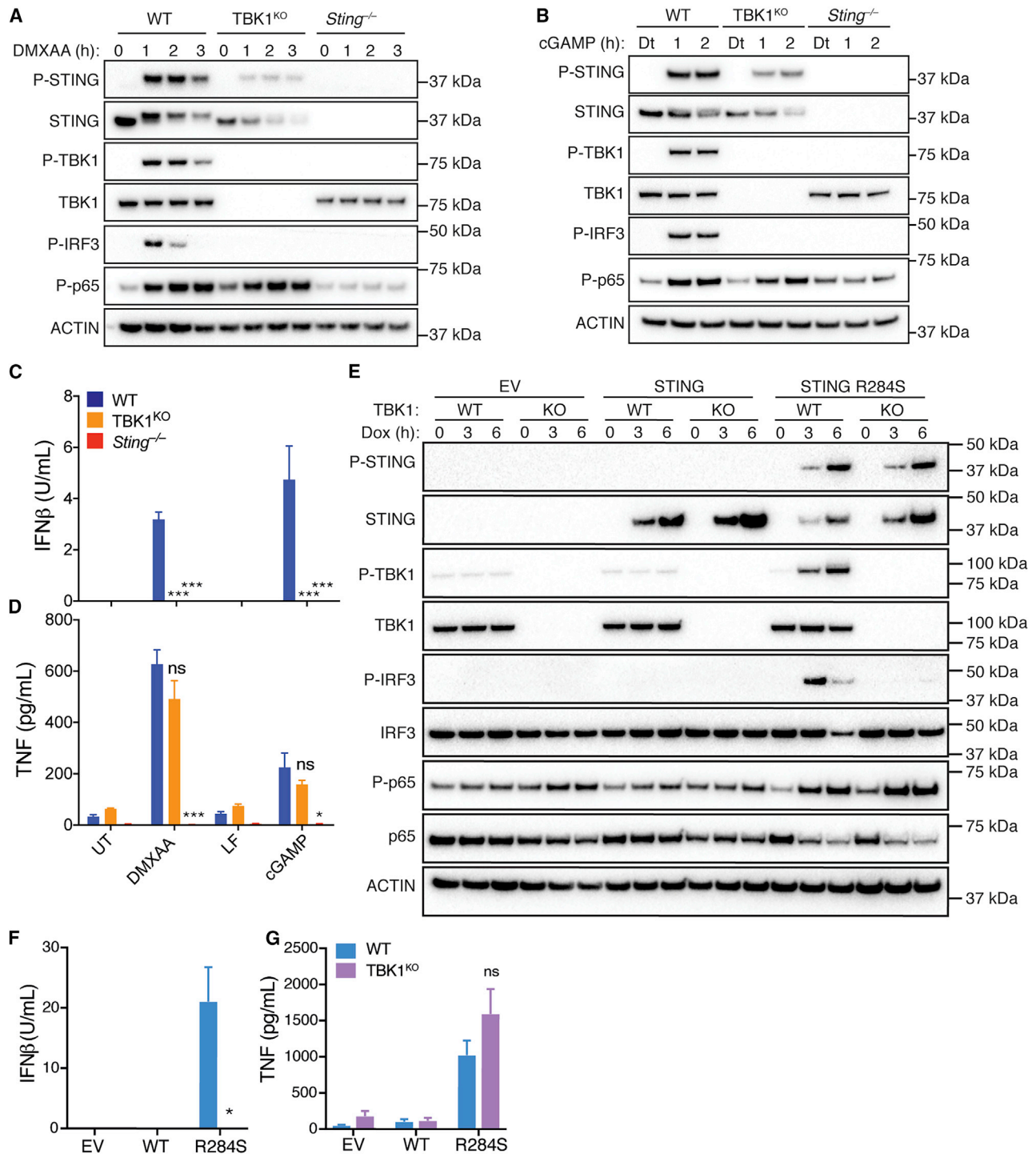
Figure 3. TBK1 Is Dispensable for NF-κB Activation Downstream of STING

(A and B) WT, TBK1[KO], and *Sting*^{−/−} iBMDMs were left untreated (0) or stimulated with 50 μg/mL DMXAA (A) or 10 μg/mL 2′3′-cGAMP in digitonin reagent (Dt) or Dt alone (B) as shown, before cells were lysed for immunoblotting with the indicated antibodies. Data are representative of at least three independent experiments.

(C and D) WT, TBK1[KO], and *Sting*^{−/−} iBMDMs were left untreated (UT) or stimulated with 50 μg/mL DMXAA or 10 μg/mL 2′3′-cGAMP in lipofectamine (LF) or LF alone for 6 h before cell supernatants were collected to measure levels of secreted IFNβ (C) and TNF (D) by ELISA. Data represent the mean from three combined experiments + SEM. *p < 0.05, ***p < 0.001, not significant (ns) compared with WT cells as determined by unpaired Student's t test.

(legend continued on next page)

kinetics (up to 3 h) following WEHI-112 pre-treatment at two doses. In the presence of WEHI-112, we observed a substantial dose-dependent reduction in p-IRF3 following STING activation (Figures 5A and 5B). Conversely, robust STING-induced NF-κB activation, indicated by increased p-p65 and reduced IκBα, was maintained over time in the presence of WEHI-112, albeit with slightly delayed kinetics (Figures 5A and 5B).

To examine the role of IKKε kinase activity in the complete absence of TBK1, we next performed experiments where we treated TBK1^{KO} iBMDMs with WEHI-112. In TBK1^{KO} iBMDMs, IKKε was activated (p-IKKε), which was also observed in the presence of WEHI-112 (Figures S3B and S3C), as previously reported (Louis et al., 2019). In WEHI-112 pre-treated cells, no differences were seen in the level of p-p65 in response to either DMXAA or 2'3'-cGAMP (Figures S3B and S3C). Consistent with this, TNF expression was similar between Ctrl and WEHI-112-treated TBK1^{KO} cells upon STING activation (Figure S3D). We then used immunofluorescence to monitor the nuclear translocation of IRF3 and NF-κB p65 in response to 2'3'-cGAMP stimulation in the presence or absence of WEHI-112 (Figures 5C and 5D). Quantification of the nuclear intensity of IRF3 revealed a significant reduction in translocation between Ctrl and WEHI-112-treated cells, whereas NF-κB p65 showed no difference (Figure 5E), indicating NF-κB nuclear translocation was not perturbed. In line with defective IRF3 nuclear translocation upon STING activation, we observed significantly blunted Ifnb1 expression and IFNβ secretion in the presence of WEHI-112 in DMXAA-treated cells (Figures 5F and 5G). Meanwhile, NF-κB-dependent TNF levels were less sensitive to WEHI-112 treatment, showing only minor reductions (Figures 5H and 5I). Similar results were seen when BMDMs were stimulated with 2'3'-cGAMP or infected with HSV-1 following WEHI-112 pre-treatment, compared with Ctrl (Figures 5J–5M). Of note, HSV-1-induced IFNβ and TNF responses were entirely dependent on STING expression in this experimental system (Figures S4A and S4B). Consistently, comparable observations using the TBK1/IKKε inhibitor, BX-795, prior to STING activation with bacterial CDNs were reported by Blaauboer et al. (2014).

Gram-positive bacterial species Listeria monocytogenes is known to induce a STING-dependent type I IFN response driven through the recognition of both bacterial DNA and CDNs by cGAS and STING, respectively (Marinho et al., 2017). Therefore, we next examined NF-κB responses downstream of Listeria monocytogenes infection in BMDMs from Tmem173$^{+/+}$ (referred to here as Sting$^{+/+}$) and Sting$^{-/-}$ mice. Both Sting$^{+/+}$ and Sting$^{-/-}$ exhibited a robust increase in p-p65 at the signaling level, as well as normal Tnf expression, in the presence of WEHI-112 upon Listeria infection (Figures S4C and S4D), demonstrating that under these experimental conditions, NF-κB activation occurs independently of STING. Comparatively, the expression of Ifnb1

was highly dependent on STING expression and, similar to our previous findings, was substantially reduced in the presence of WEHI-112 (Figure S4E).

Because TBK1 and IKKε kinase inhibition was critical for type I IFN production but dispensable for cGAS-STING-induced NF-κB activation in mouse macrophages, we also wanted to determine whether the same was true of human immune cells. To do this, we isolated peripheral blood mononuclear cells (PBMCs) from healthy human donors and pre-treated them with WEHI-112 before stimulating cells with the cyclic-di-AMP analog, 2'3'-CDA (PS)2 (RR), or with transfected HT-DNA. Consistent with our results from mouse macrophages, compared with Ctrl, we observed a dose-dependent reduction in STING-induced IFNB1 expression upon WEHI-112 treatment (Figure 5N). In contrast, there was little difference in TNF expression with WEHI-112 pre-treatment upon STING activation (Figure 5O). We then used our doxycycline-inducible lentiviral system to express WT STING, STING R284S, or an EV Ctrl in human THP-1 monocytes. As in WT iBMDMs, overexpression of WT STING failed to induce phosphorylation of STING, or any downstream signaling components, whereas expression of STING R284S led to robust phosphorylation of STING, TBK1, IRF3, and NF-κB p65 (Figure 5P). In addition, only expression of STING R284S resulted in significant downstream induction of IFNB1, IRF7, TNF, and IL1B inflammatory genes (Figures S4F–S4I). Importantly, pre-treatment of these THP-1 monocytes with two different doses of WEHI-112 prior to doxycycline-induced STING R284S expression markedly decreased IFNB1 expression in a dose-dependent manner (Figure 5Q). Conversely, there was no change in TNF expression between vehicle Ctrl or WEHI-112-treated THP-1 monocytes expressing STING R284S (Figure 5R).

Taken together, these data strongly suggest that downstream of cGAS-STING, the activation of IRF3 and subsequent production of IFNβ are exquisitely reliant on the kinase activities of TBK1 and IKKε, whereas NF-κB-dependent cytokine responses are less so.

TAK1 and IKKβ, but Not TRAF6, Are Required for STING-NF-κB Responses

The E3 ubiquitin (Ub) ligase TNF receptor-associated factor 6 (TRAF6) is well known to drive NF-κB downstream of TLR activation (Balka and De Nardo, 2019) and has also been implicated in both canonical and non-canonical STING-mediated activation of NF-κB in response to dsDNA and nuclear DNA damage, respectively (Abe and Barber, 2014; Dunphy et al., 2018). In fact, recently, STING-mediated NF-κB responses in zebrafish, but not humans, were shown to be enhanced via interactions with TRAF6 (de Oliveira Mann et al., 2019). Hence we generated iBMDMs deficient in TRAF6 (TRAF6^{KO}) and tested their ability to activate NF-κB in response to STING activation. Both DMXAA- and 2'3'-cGAMP-induced STING signaling, including increased

---

(E) WT and TBK1^{KO} iBMDMs stably transduced with either an empty vector (EV) Ctrl, WT STING, or STING R284S were left untreated (0) or treated with 1 μg/mL doxycycline for 3 and 6 h in order to induce protein expression. Cells were then lysed for immunoblotting with the indicated antibodies. Data are representative of three independent experiments.

(F and G) Cell supernatants were collected after 6 h of 1 μg/mL doxycycline to measure levels of secreted IFNβ (F) and TNF (G) by ELISA. Data represent the mean from three combined experiments + SEM. *p < 0.05, not significant (ns) compared with WT iBMDMs as determined by unpaired Student's t test.
See also Figure S2.
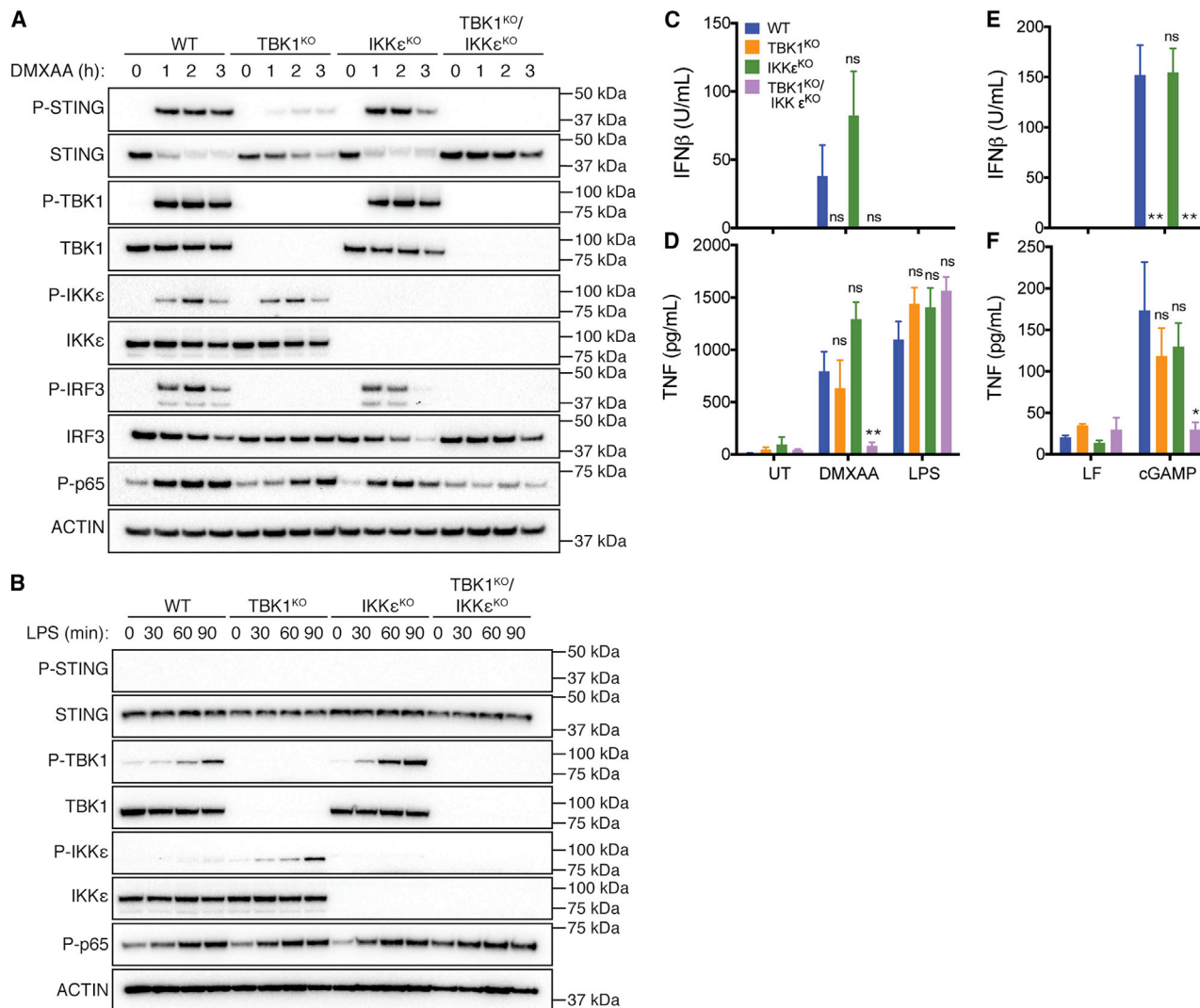
**Figure 4. STING Activates NF-κB in a TBK1/IKKε Redundant Manner**

(A and B) WT, TBK1[KO], IKKε[KO], and TBK1[KO]/IKKε[KO] iBMDMs were left untreated (0) or stimulated with 50 μg/mL DMXAA (A) or 200 ng/mL LPS (B) as shown, before cells were lysed for immunoblotting with the indicated antibodies. Data are representative of three independent experiments.

(C–F) WT, TBK1[KO], IKKε[KO], and TBK1[KO]/IKKε[KO] iBMDMs were left untreated (UT) or stimulated with 50 μg/mL DMXAA, 200 ng/mL LPS (C and D), or 10 μg/mL 2′3′-cGAMP in lipofectamine (LF) or LF alone (E and F) for 6 h before cell supernatants were collected to measure levels of secreted IFNβ (C and E) and TNF (D and F) by ELISA. Data represent the mean from three combined experiments + SEM. *p < 0.05, **p < 0.01, not significant (ns) compared with WT cells as determined by unpaired Student's t test.

p-p65 and loss of IκBα, were equivalent in both WT and TRAF6[KO] iBMDMs, whereas in contrast, TLR9 (CpG DNA)-dependent NF-κB responses were ablated in TRAF6-deficient macrophages (Figures 6A and 6B). Consistently, secretion of TNF following DMXAA or 2′3′-cGAMP stimulation was also similar in WT and TRAF6[KO] iBMDMs (Figure 6C). In contrast, but as expected, TNF production was completely lost in cells lacking TRAF6 in response to TLR9 or TLR2 (P3C) activation (Figure 6C). These findings demonstrate that although TRAF6 is critically required for TLR responses, it is not required for canonical NF-κB activation during STING signaling.

In order to investigate further how NF-κB is activated downstream of STING activation, we examined the role of putative up-

stream transforming growth factor β-activated kinase 1 (TAK1) and the IKK signaling complexes via pharmacological inhibition. We pre-treated BMDMs with a vehicle Ctrl (DMSO), an IKKβ kinase inhibitor (TPCA-1), or a TAK1 kinase inhibitor (5z-7-Oxozeaenol) before stimulating cells with either DMXAA or 2′3′-cGAMP (Figures 6D and 6E). Inhibition of IKKβ or TAK1 kinase activity significantly reduced levels of p-p65 and the loss of IκBα (Figures 6D and 6E). In contrast, p-STING and p-TBK1 were only minimally affected by IKKβ kinase inhibition, although p-IRF3 was reduced, as previously reported in cells depleted of IKKβ (Fang et al., 2017). We also noted that TAK1 kinase inhibition modestly reduced p-STING, p-IRF3, and p-TBK1 levels (Figures 6D and 6E). However, these differences are unlikely to
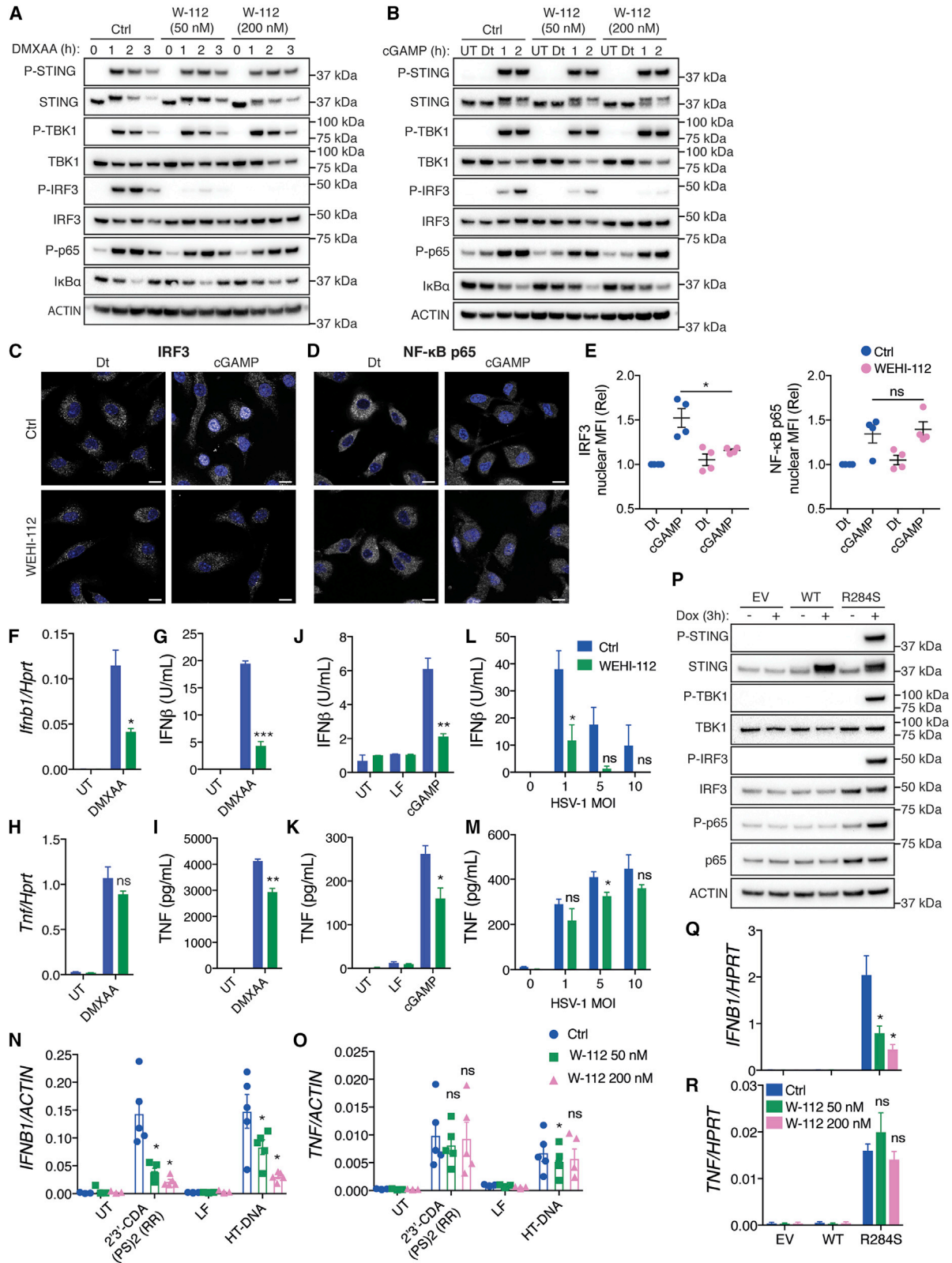
(legend on next page)

account for the reductions observed in STING-induced p-p65 following TAK1 inhibition. These data strongly suggest that the IKKβ and TAK1 complexes are activated downstream of STING-induced TBK1 and IKKε activity. Of note, TAK1 kinase inhibition strongly inhibited STING-dependent phosphorylation of IKKα and IKKβ, further suggesting that TAK1 acts upstream of the IKK complex (Figures 6D and 6E). Similar results were obtained following stimulation of TLR9 with CpG DNA, which is known to activate IKKβ- and TAK1-dependent NF-κB activation. Together, these data demonstrate that STING activation elicits the kinase activities of both TAK1 and IKKβ to drive subsequent NF-κB responses.

DISCUSSION

The cGAS-STING pathway comprises a major component of the host innate immune response to viral infection. Beyond this, it has also been implicated as a key player in a number of cellular and disease processes, including autoimmune disease, autoinflammatory conditions, neurodegenerative disorders, and cancer. Due to the robust nature of the type I IFN response elicited via cGAS-STING, enormous focus has been placed on the mechanisms underpinning this process. However, although less studied, the NF-κB pathway is also of great importance to STING responses. It is a widely held view that TBK1 alone elicits NF-κB responses downstream of STING, but we now provide evidence that redefines the fundamental molecular mechanisms of STING-induced NF-κB signaling (Figure S5). We demonstrate that, in fact, TBK1 and IKKε act redundantly to drive NF-κB activation, whereas type I IFN responses are elicited by TBK1 and its kinase activity. We further demonstrate that phosphorylation of STING at serine 365 (366 in humans) is predominantly mediated

by kinase activity of TBK1; however, residual phosphorylation at this site occurs in the absence of TBK1, through IKKε. In contrast, activation of STING-induced NF-κB activation appears significantly less dependent on the kinase activities of TBK1 and IKKε. Of note, the TBK1/IKKε redundant mechanism appears specific to STING-mediated NF-κB signaling, as we (Figure 4) and others have shown that TLRs, as well as IL-1β and TNF signaling, drive NF-κB responses in a TBK1- and IKKε-independent manner (Clark et al., 2009; Hemmi et al., 2004; Perry et al., 2004). Downstream of STING and TBK1/IKKε, we further show that the TAK1 and IKK complexes drive canonical NF-κB responses and the production of pro-inflammatory cytokines (Figure 6 and Figure S5).

Our revised model of STING signaling has important implications regarding the clinical efficacy of therapies targeting STING-related responses. To date, suggested therapies for numerous autoimmune and autoinflammatory diseases, especially in the group of type I interferonopathies, has involved targeting IFN pathways. TBK1 has been postulated as a potential therapeutic target for treating such diseases (Hasan and Yan, 2016). Our findings demonstrate that TBK1 kinase inhibition may not lead to complete control of STING-driven pathology and broader type I interferonopathies. However, TBK1/IKKε inhibitors may still provide health benefits for a number of diseases related to STING activation, including TREX1-mediated autoimmunity (Hasan et al., 2015). For example, the cGAS-STING pathway is heavily implicated in the development of autoimmunity (e.g., Aicardi-Goutières syndrome and forms of lupus) in humans and mice lacking the DNA degrading exonuclease DNase III (also known as TREX1). Indeed, the pathology of $Trex1^{-/-}$ mice is completely rescued by crossing these animals to either IFNAR (the receptor for type I IFNs)- or STING-deficient mice (Gall et al.,

Figure 5. STING-Induced NF-κB Activity Is Less Sensitive to TBK1/IKKε Kinase Inhibition Than Type I IFN Responses

(A and B) Primary BMDMs were pre-treated with either a DMSO vehicle Ctrl or 50 and 200 nM WEHI-112 (TBK1/IKKε kinase inhibitor) for 1 h prior to stimulation with 50 μg/mL DMXAA (A) or 10 μg/mL 2′3′-cGAMP in digitonin reagent (Dt) or Dt alone (B) as shown, before cells were lysed for immunoblotting with the indicated antibodies. Data are representative of at least three independent experiments.

(C–E) Primary BMDMs were pre-treated with either a DMSO vehicle Ctrl or 200 nM WEHI-112 for 1 h and then stimulated with 10 μg/mL 2′3′-cGAMP in digitonin reagent (Dt) or Dt alone for 4 h before fixation and staining for IRF3 (C) or NF-κB p65 (D) and nuclei (shown in blue). Samples were then examined by confocal microscopy. Representative images are presented from four biological replicates (C and D). Scale bars, 10 μm. (E) IRF3 and NF-κB p65 nuclear translocation was then quantified by examining the mean fluorescence intensity. Data represent the mean from four biological replicates ± SEM. *p < 0.05, not significant (ns) compared with Ctrl as determined by unpaired Student's t test.

(F–I) Primary BMDMs were pre-treated with either a DMSO vehicle Ctrl or 50 nM WEHI-112 for 1 h prior and then left untreated (UT) or stimulated with 50 μg/mL DMXAA for 4 h before cells were lysed for RNA isolation and *Ifnb1* (F) and *Tnf* (H) gene expression analysis by qPCR, and cell supernatants were collected to measure levels of secreted IFNβ (G) and TNF (I) by ELISA. Data represent the mean from three combined experiments + SEM. *p < 0.05, **p < 0.01, ***p < 0.001, not significant (ns) compared with Ctrl as determined by unpaired Student's t test.

(J–M) Primary BMDMs were pre-treated with either a DMSO vehicle Ctrl or 50 nM WEHI-112 for 1 h prior and then left untreated (UT/0) or stimulated with 10 μg/mL 2′3′-cGAMP in lipofectamine (LF) or LF alone (J and K), or infected with HSV-1 as indicated (L and M) for 4 h, before cell supernatants were collected to measure levels of secreted IFNβ (J and L) and TNF (K and M) by ELISA. Data represent the mean from three combined experiments + SEM. *p < 0.05, **p < 0.01, not significant (ns) compared with Ctrl as determined by unpaired Student's t test.

(N and O) Fresh human peripheral blood mononuclear cells (PBMCs) were pre-treated with either a DMSO vehicle Ctrl, 50 nM WEHI-112, or 200 nM WEHI-112 for 1 h and then left untreated (UT) or stimulated with 20 μM 2′3′-cyclic di-AMP (CDA) (PS)2 (RR) added directly to the media, HT-DNA in lipofectamine (LF), or LF alone for 16 h before analysis of *IFNB1* (N) and *TNF* (O) gene expression by qPCR. Data represent the mean of five combined human donor samples ± SEM. *p < 0.05, not significant (ns) compared with Ctrl as determined by paired Student's t test.

(P) THP-1 monocytic-like cells stably transduced with either an empty vector (EV) Ctrl, WT STING, or STING R284S were left untreated (–) or treated with 1 μg/mL doxycycline for 3 h (+) in order to induce protein expression. Cells were then lysed for immunoblotting with the indicated antibodies. Data are representative of three independent experiments.

(Q and R) THP-1 monocytic cells stably transduced with either an empty vector (EV) Ctrl, WT STING, or STING R284S were pre-treated with 50 or 200 nM WEHI-112 before treatment with 1 μg/mL doxycycline for 6 h. Cells were lysed, and RNA was isolated before analysis of *IFNB1* (Q) and *TNF* (R) gene expression by qPCR. Data represent the mean from three combined experiments + SEM. *p < 0.05, not significant (ns) compared with Ctrl as determined by unpaired Student's t test.

See also Figures S3 and S4.
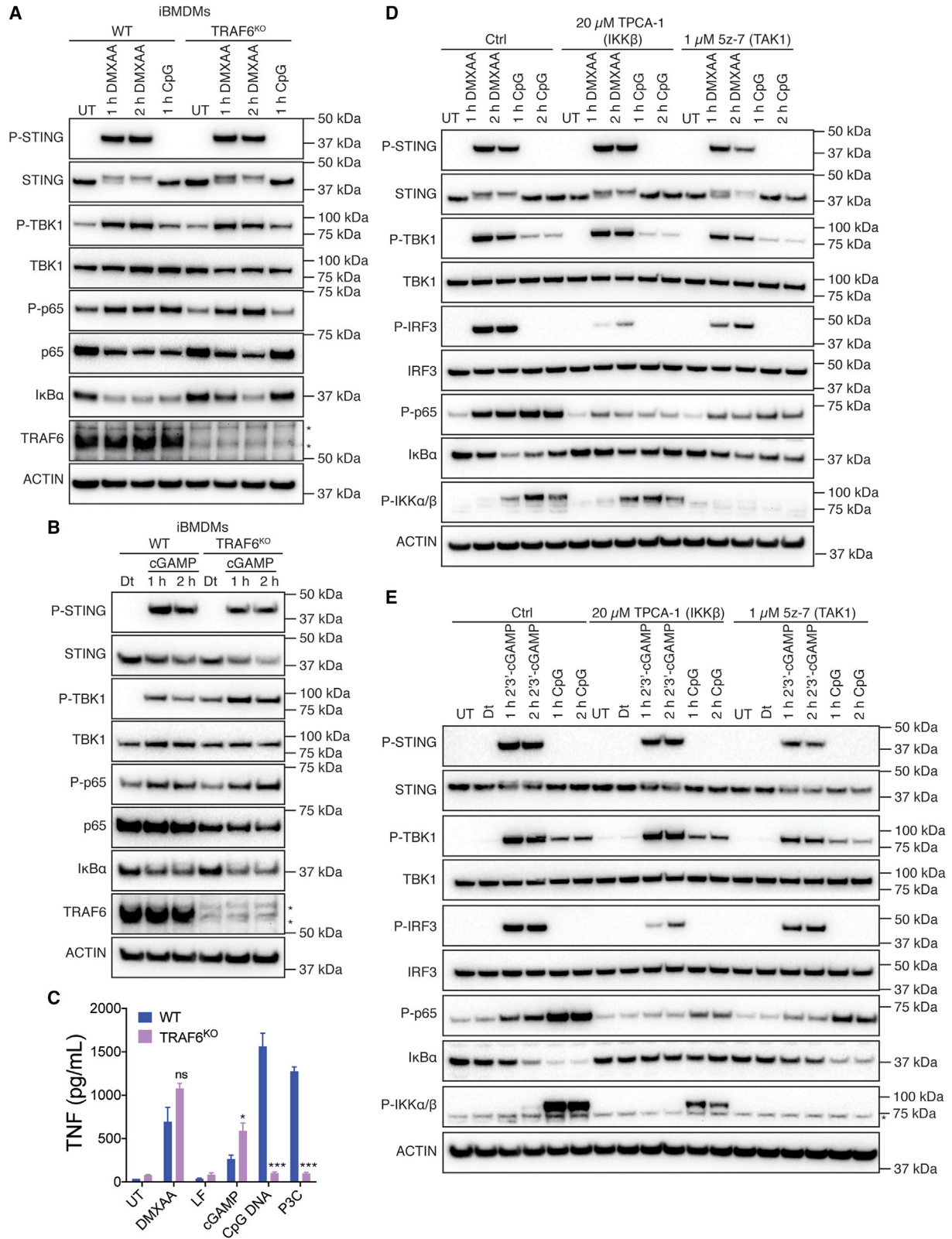
(legend on next page)

2012; Stetson et al., 2008). Furthermore, targeted TBK1/IKKε inhibition could be beneficial against certain bacterial infections that create a protective niche by exploiting STING-mediated type I IFNs, such as *Listeria monocytogenes* (Marinho et al., 2017). In this context, TBK1/IKKε inhibitors would effectively reduce type I IFNs, thereby redirecting the host's cellular response to a primarily NF-κB-driven, anti-bacterial inflammatory state.

Diseases driven by aberrant cGAS-STING activation can display pathologies independent of type I IFNs. For instance, DNaseII-mediated autoimmunity that manifests as chronic polyarthritis is driven by a strong pro-inflammatory cytokine response that can be rescued by crossing *DnaseII*−/− mice to those lacking cGAS or STING (Ahn et al., 2012; Gao et al., 2015), but not IFNAR (Kawane et al., 2006, 2010). Likewise, murine models of SAVI have demonstrated potentially significant roles for non-IFN signaling downstream of STING autoactivation. Namely, when STING gain-of-function mice were crossed onto an *Irf3*−/− background, animals retained perivascular pulmonary inflammation, myeloid cell expansion, and T cell cytopenia, suggesting that other STING-induced pathways may play a key role in disease pathogenesis (Warner et al., 2017). In line with this finding, several recent studies observed that when STING N153S or V154M gain-of-function mice were crossed to IRF3- or IFNAR-deficient mice, the SAVI phenotype (e.g., lung disease) ensued independently of the type I IFN pathway (Luksch et al., 2019; Motwani et al., 2019). Moreover, IFNAR-deficient STING gain-of-function mice were actually found to exhibit significant lung and kidney inflammation (Bouis et al., 2019). In the context of SAVI patients, targeting the signaling pathway downstream of IFNAR via JAK inhibition has shown the greatest efficacy; however, in some reported cases, significant disease-associated pathologies have persisted in spite of treatment (Saldanha et al., 2018; Sanchez et al., 2018). Ultimately, this suggests the clinical scope of TBK1/IKKε kinase inhibition in cGAS-STING pathology needs to be carefully considered. In this regard, the recent development of small-molecule compounds directly inhibiting cGAS or STING may have greater potential for clinical translation. Indeed, administration of specific cGAS and STING antagonists was recently shown to significantly diminish inflammation and disease pathologies in the *Trex1*−/− mouse model (An et al., 2018; Haag et al., 2018). It would be of great interest to evaluate the efficacy of such compounds in SAVI mice and other disease models that display non-IFN-dependent pathologies.

STING agonists have also emerged as a major therapeutic target for cancer immunotherapy, with several molecules currently in phase I clinical trials (Zhu and Li, 2018). It is well known that endogenous type I IFNs are beneficial in limiting cancer progression by priming T cells and driving anti-cancer immune responses (Zitvogel et al., 2015). For instance, IFNAR signaling has been shown to be critical for STING-mediated tumor suppression in murine models of melanoma (Corrales et al., 2015; Demaria et al., 2015). However, the role of STING-induced NF-κB in cancer is not well defined. Of potential benefit, NF-κB can synergize with IRF3 to increase maximal expression of IFNβ. On the other hand, it is well described that NF-κB can be constitutively activated in cancer cells driving tumor initiation and metastasis, as well as promoting cell survival and proliferation (Taniguchi and Karin, 2018). Hence a number of anti-cancer agents target components of NF-κB signaling (Baud and Karin, 2009). The ability of STING to activate NF-κB may therefore diminish the full potential of STING agonists for anti-cancer therapy. As such, STING activation in combination with reduced NF-κB activity could provide synergistic benefit for tumor immunotherapy. Therefore, studies more closely examining the role of STING-induced NF-κB in murine models of cancer would also be of great interest.

In summary, our work identifies the molecular mechanisms underpinning NF-κB activation by STING, distinguishing this pathway from IRF3-mediated type I IFN responses. These findings prompt future research questions regarding the regulation of signaling events downstream of STING and have further implications regarding therapeutic targeting of STING-related diseases and cancer immunotherapy.

STAR★METHODS

Detailed methods are provided in the online version of this paper and include the following:

- KEY RESOURCES TABLE
- LEAD CONTACT AND MATERIALS AVAILABILITY
- EXPERIMENTAL MODEL AND SUBJECT DETAILS
  - Animals
  - Primary murine and human immune cells
  - Immortalized cell lines
  - *Sting*−/− immortalized BMDMs (iBMDMs)
  - Gene knockout cells via CRISPR/Cas9
- METHOD DETAILS

Figure 6. STING-Induced NF-κB Responses Require TAK1 and IKKβ Activity, but Not TRAF6

(A and B) WT and TRAF6KO iBMDMs were left untreated (UT) or stimulated with 50 μg/mL DMXAA (A), 20 μg/mL 2′3′-cGAMP in digitonin reagent (Dt) or Dt alone (B), or 1 μM CpG DNA (A) as indicated, before cells were lysed for immunoblotting with the indicated antibodies. Asterisks indicate non-specific bands. Data are representative of at least three independent experiments.

(C) WT and TRAF6KO iBMDMs were left untreated (UT) or stimulated with 50 μg/mL DMXAA, 10 μg/mL 2′3′-cGAMP in lipofectamine (LF) or LF alone, 1 μM CpG DNA, or 500 ng/mL Pam3CysK4 (P3C) for 6 h before cell supernatants were collected to measure levels of secreted TNF by ELISA. Data represent the mean from three combined experiments + SEM. *p < 0.05, ***p < 0.001, not significant (ns) compared with WT cells as determined by unpaired Student's t test.

(D and E) Primary BMDMs were pre-treated with either a DMSO vehicle Ctrl, 20 μM TPCA-1 (IKKβ inhibitor), or 1 μM 5z-7 (TAK1 inhibitor) and then left untreated (UT) or stimulated with 50 μg/mL DMXAA (D), 10 μg/mL 2′3′-cGAMP in digitonin reagent (Dt) or Dt alone (E), or 1 μM CpG DNA (D and E) as indicated, before cells were lysed for immunoblotting with the indicated antibodies. Asterisk indicates a non-specific band (E). Data are representative of at least three independent experiments.

- ○ Generation of lentiviral plasmids
- ○ Lentiviral transduction
- ○ Preparation of whole-cell lysates (WCLs)
- ○ Immunoblotting
- ○ Quantitative real time-PCR
- ○ Enzyme-Linked Immunosorbent Assay (ELISA)
- ○ Immunofluorescence
- QUANTIFICATION AND STATISTICAL ANALYSIS
- DATA AND CODE AVAILABILITY

SUPPLEMENTAL INFORMATION

Supplemental Information can be found online at https://doi.org/10.1016/j.celrep.2020.03.056.

ACKNOWLEDGMENTS

AUTHOR CONTRIBUTIONS

DECLARATION OF INTERESTS

REFERENCES

Abe, T., and Barber, G.N. (2014). Cytosolic-DNA-mediated, STING-dependent proinflammatory gene induction necessitates canonical NF-κB activation through TBK1. J. Virol. 88, 5328–5341.

Ablasser, A., Goldeck, M., Cavlar, T., Deimling, T., Witte, G., Röhl, I., Hopfner, K.P., Ludwig, J., and Hornung, V. (2013). cGAS produces a 2′-5′-linked cyclic dinucleotide second messenger that activates STING. Nature 498, 380–384.

Ablasser, A., Hemmerling, I., Schmid-Burgk, J.L., Behrendt, R., Roers, A., and Hornung, V. (2014). TREX1 deficiency triggers cell-autonomous immunity in a cGAS-dependent manner. J. Immunol. 192, 5993–5997.

Ahn, J., Gutman, D., Saijo, S., and Barber, G.N. (2012). STING manifests self DNA-dependent inflammatory disease. Proc. Natl. Acad. Sci. USA 109, 19386–19391.

An, J., Woodward, J.J., Lai, W., Minie, M., Sun, X., Tanaka, L., Snyder, J.M., Sasaki, T., and Elkon, K.B. (2018). Inhibition of Cyclic GMP-AMP Synthase Using a Novel Antimalarial Drug Derivative in Trex1-Deficient Mice. Arthritis Rheumatol. 70, 1807–1819.

Baker, P.J., and Masters, S.L. (2018). Generation of Genetic Knockouts in Myeloid Cell Lines Using a Lentiviral CRISPR/Cas9 System. Methods Mol. Biol. 1714, 41–55.

Baker, P.J., De Nardo, D., Moghaddas, F., Tran, L.S., Bachem, A., Nguyen, T., Hayman, T., Tye, H., Vince, J.E., Bedoui, S., et al. (2017). Posttranslational Modification as a Critical Determinant of Cytoplasmic Innate Immune Recognition. Physiol. Rev. 97, 1165–1209.

Balka, K.R., and De Nardo, D. (2019). Understanding early TLR signaling through the Myddosome. J. Leukoc. Biol. 105, 339–351.

Baud, V., and Karin, M. (2009). Is NF-kappaB a good target for cancer therapy? Hopes and pitfalls. Nat. Rev. Drug Discov. 8, 33–40.

Blaauboer, S.M., Gabrielle, V.D., and Jin, L. (2014). MPYS/STING-mediated TNF-α, not type I IFN, is essential for the mucosal adjuvant activity of (3′-5′)-cyclic-di-guanosine-monophosphate in vivo. J. Immunol. 192, 492–502.

Bonnard, M., Mirtsos, C., Suzuki, S., Graham, K., Huang, J., Ng, M., Itié, A., Wakeham, A., Shahinian, A., Henzel, W.J., et al. (2000). Deficiency of T2K leads to apoptotic liver degeneration and impaired NF-kappaB-dependent gene transcription. EMBO J. 19, 4976–4985.

Bouis, D., Kirstetter, P., Arbogast, F., Lamon, D., Delgado, V., Jung, S., Ebel, C., Jacobs, H., Knapp, A.M., Jeremiah, N., et al. (2019). Severe combined immunodeficiency in stimulator of interferon genes (STING) V154M/wild-type mice. J. Allergy Clin. Immunol. 143, 712–725.e715.

Burdette, D.L., Monroe, K.M., Sotelo-Troha, K., Iwig, J.S., Eckert, B., Hyodo, M., Hayakawa, Y., and Vance, R.E. (2011). STING is a direct innate immune sensor of cyclic di-GMP. Nature 478, 515–518.

Cardona Gloria, Y., Latz, E., and De Nardo, D. (2018). Generation of Innate Immune Reporter Cells Using Retroviral Transduction. Methods Mol. Biol. 1714, 97–117.

Cerboni, S., Jeremiah, N., Gentili, M., Gehrmann, U., Conrad, C., Stolzenberg, M.C., Picard, C., Neven, B., Fischer, A., Amigorena, S., et al. (2017). Intrinsic antiproliferative activity of the innate sensor STING in T lymphocytes. J. Exp. Med. 214, 1769–1785.

Chen, H., Pei, R., Zhu, W., Zeng, R., Wang, Y., Wang, Y., Lu, M., and Chen, X. (2014). An alternative splicing isoform of MITA antagonizes MITA-mediated induction of type I IFNs. J. Immunol. 192, 1162–1170.

Clark, K., Plater, L., Peggie, M., and Cohen, P. (2009). Use of the pharmacological inhibitor BX795 to study the regulation and physiological roles of TBK1 and IkappaB kinase epsilon: a distinct upstream kinase mediates Ser-172 phosphorylation and activation. J. Biol. Chem. 284, 14136–14146.

Clarke, S.L., Pellowe, E.J., de Jesus, A.A., Goldbach-Mansky, R., Hilliard, T.N., and Ramanan, A.V. (2016). Interstitial Lung Disease Caused by STING-associated Vasculopathy with Onset in Infancy. Am. J. Respir. Crit. Care Med. 194, 639–642.

Corrales, L., Glickman, L.H., McWhirter, S.M., Kanne, D.B., Sivick, K.E., Katibah, G.E., Woo, S.R., Lemmens, E., Banda, T., Leong, J.J., et al. (2015). Direct Activation of STING in the Tumor Microenvironment Leads to Potent and Systemic Tumor Regression and Immunity. Cell Rep. 11, 1018–1030.

De Nardo, D. (2017). Activation of the Innate Immune Receptors: Guardians of the Micro Galaxy: Activation and Functions of the Innate Immune Receptors. Adv. Exp. Med. Biol. 1024, 1–35.

De Nardo, D., Balka, K.R., Cardona Gloria, Y., Rao, V.R., Latz, E., and Masters, S.L. (2018a). Interleukin-1 receptor-associated kinase 4 (IRAK4) plays a dual role in myddosome formation and Toll-like receptor signaling. J. Biol. Chem. 293, 15195–15207.

De Nardo, D., Kalvakolanu, D.V., and Latz, E. (2018b). Immortalization of Murine Bone Marrow-Derived Macrophages. Methods Mol. Biol. 1784, 35–49.

de Oliveira Mann, C.C., Orzalli, M.H., King, D.S., Kagan, J.C., Lee, A.S.Y., and Kranzusch, P.J. (2019). Modular architecture of the STING C-terminal tail allows interferon and NF-κB signaling adaptation. Cell Rep. 27, 1165–1175.e1165.

Demaria, O., De Gassart, A., Coso, S., Gestermann, N., Di Domizio, J., Flatz, L., Gaide, O., Michielin, O., Hwu, P., Petrova, T.V., et al. (2015). STING activation of tumor endothelial cells initiates spontaneous and therapeutic antitumor immunity. Proc. Natl. Acad. Sci. USA 112, 15408–15413.

Diner, E.J., Burdette, D.L., Wilson, S.C., Monroe, K.M., Kellenberger, C.A., Hyodo, M., Hayakawa, Y., Hammond, M.C., and Vance, R.E. (2013). The innate immune DNA sensor cGAS produces a noncanonical cyclic dinucleotide that activates human STING. Cell Rep. 3, 1355–1361.

Dunphy, G., Flannery, S.M., Almine, J.F., Connolly, D.J., Paulus, C., Jønsson, K.L., Jakobsen, M.R., Nevels, M.M., Bowie, A.G., and Unterholzner, L. (2018). Non-canonical activation of the DNA sensing adaptor STING by ATM and IFI16 mediates NF-κB signaling after nuclear DNA damage. Mol. Cell 71, 745–760.e745.

Fang, R., Wang, C., Jiang, Q., Lv, M., Gao, P., Yu, X., Mu, P., Zhang, R., Bi, S., Feng, J.M., and Jiang, Z. (2017). NEMO-IKKβ Are Essential for IRF3 and NF-κB Activation in the cGAS-STING Pathway. J. Immunol. 199, 3222–3233.

Gall, A., Treuting, P., Elkon, K.B., Loo, Y.M., Gale, M., Jr., Barber, G.N., and Stetson, D.B. (2012). Autoimmunity initiates in nonhematopoietic cells and progresses via lymphocytes in an interferon-dependent autoimmune disease. Immunity 36, 120–131.

Gao, D., Li, T., Li, X.D., Chen, X., Li, Q.Z., Wight-Carter, M., and Chen, Z.J. (2015). Activation of cyclic GMP-AMP synthase by self-DNA causes autoimmune diseases. Proc. Natl. Acad. Sci. USA 112, E5699–E5705.

Gkirtzimanaki, K., Kabrani, E., Nikoleri, D., Polyzos, A., Blanas, A., Sidiropoulos, P., Makrigiannakis, A., Bertsias, G., Boumpas, D.T., and Verginis, P. (2018). IFNalpha Impairs Autophagic Degradation of mtDNA Promoting Autoreactivity of SLE Monocytes in a STING-Dependent Fashion. Cell Rep. 25, 921–933.e5.

Haag, S.M., Gulen, M.F., Reymond, L., Gibelin, A., Abrami, L., Decout, A., Heymann, M., van der Goot, F.G., Turcatti, G., Behrendt, R., and Ablasser, A. (2018). Targeting STING with covalent small-molecule inhibitors. Nature 559, 269–273.

Hasan, M., Dobbs, N., Khan, S., White, M.A., Wakeland, E.K., Li, Q.Z., and Yan, N. (2015). Cutting Edge: Inhibiting TBK1 by Compound II Ameliorates Autoimmune Disease in Mice. J. Immunol. 195, 4573–4577.

Hasan, M., and Yan, N. (2016). Therapeutic potential of targeting TBK1 in autoimmune diseases and interferonopathies. Pharmacol. Res. 111, 336–342.

Hemmi, H., Takeuchi, O., Sato, S., Yamamoto, M., Kaisho, T., Sanjo, H., Kawai, T., Hoshino, K., Takeda, K., and Akira, S. (2004). The roles of two IkappaB kinase-related kinases in lipopolysaccharide and double stranded RNA signaling and viral infection. J. Exp. Med. 199, 1641–1650.

Ishikawa, H., and Barber, G.N. (2008). STING is an endoplasmic reticulum adaptor that facilitates innate immune signalling. Nature 455, 674–678.

Ishikawa, H., Ma, Z., and Barber, G.N. (2009). STING regulates intracellular DNA-mediated, type I interferon-dependent innate immunity. Nature 461, 788–792.

Kawane, K., Ohtani, M., Miwa, K., Kizawa, T., Kanbara, Y., Yoshioka, Y., Yoshikawa, H., and Nagata, S. (2006). Chronic polyarthritis caused by mammalian DNA that escapes from degradation in macrophages. Nature 443, 998–1002.

Kawane, K., Tanaka, H., Kitahara, Y., Shimaoka, S., and Nagata, S. (2010). Cytokine-dependent but acquired immunity-independent arthritis caused by DNA escaped from degradation. Proc. Natl. Acad. Sci. USA 107, 19432–19437.

Konno, H., Konno, K., and Barber, G.N. (2013). Cyclic dinucleotides trigger ULK1 (ATG1) phosphorylation of STING to prevent sustained innate immune signaling. Cell 155, 688–698.

Konno, H., Chinn, I.K., Hong, D., Orange, J.S., Lupski, J.R., Mendoza, A., Pedroza, L.A., and Barber, G.N. (2018). Pro-inflammation Associated with a Gain-of-Function Mutation (R284S) in the Innate Immune Sensor STING. Cell Rep. 23, 1112–1123.

Kranzusch, P.J., Wilson, S.C., Lee, A.S., Berger, J.M., Doudna, J.A., and Vance, R.E. (2015). Ancient Origin of cGAS-STING Reveals Mechanism of Universal 2′,3′ cGAMP Signaling. Mol. Cell 59, 891–903.

Lafont, E., Draber, P., Rieser, E., Reichert, M., Kupka, S., de Miguel, D., Draberova, H., von Mässenhausen, A., Bhamra, A., Henderson, S., et al. (2018). TBK1 and IKKε prevent TNF-induced cell death by RIPK1 phosphorylation. Nat. Cell Biol. 20, 1389–1399.

Latz, E., Xiao, T.S., and Stutz, A. (2013). Activation and regulation of the inflammasomes. Nat. Rev. Immunol. 13, 397–411.

Li, X.D., Wu, J., Gao, D., Wang, H., Sun, L., and Chen, Z.J. (2013). Pivotal roles of cGAS-cGAMP signaling in antiviral defense and immune adjuvant effects. Science 341, 1390–1394.

Liu, Y., Jesus, A.A., Marrero, B., Yang, D., Ramsey, S.E., Sanchez, G.A.M., Tenbrock, K., Wittkowski, H., Jones, O.Y., Kuehn, H.S., et al. (2014). Activated STING in a vascular and pulmonary syndrome. N. Engl. J. Med. 371, 507–518.

Liu, S., Cai, X., Wu, J., Cong, Q., Chen, X., Li, T., Du, F., Ren, J., Wu, Y.T., Grishin, N.V., and Chen, Z.J. (2015). Phosphorylation of innate immune adaptor proteins MAVS, STING, and TRIF induces IRF3 activation. Science 347, aaa2630.

Louis, C., Ngo, D., D'Silva, D.B., Hansen, J., Phillipson, L., Jousset, H., Novello, P., Segal, D., Lawlor, K.E., Burns, C.J., and Wicks, I.P. (2019). Therapeutic Effects of a TANK-Binding Kinase 1 Inhibitor in Germinal Center-Driven Collagen-Induced Arthritis. Arthritis Rheumatol. 71, 50–62.

Luksch, H., Stinson, W.A., Platt, D.J., Qian, W., Kalugotla, G., Miner, C.A., Bennion, B.G., Gerbaulet, A., Rösen-Wolff, A., and Miner, J.J. (2019). STING-associated lung disease in mice relies on T cells but not type I interferon. J. Allergy Clin. Immunol. 144, 254–266.e8.

Mansouri, S., Patel, S., Katikaneni, D.S., Blaauboer, S.M., Wang, W., Schattgen, S., Fitzgerald, K., and Jin, L. (2019). Immature lung TNFR2⁻ conventional DC 2 subpopulation activates moDCs to promote cyclic di-GMP mucosal adjuvant responses in vivo. Mucosal Immunol. 12, 277–289.

Margolis, S.R., Wilson, S.C., and Vance, R.E. (2017). Evolutionary Origins of cGAS-STING Signaling. Trends Immunol. 38, 733–743.

Marinho, F.V., Benmerzoug, S., Oliveira, S.C., Ryffel, B., and Quesniaux, V.F.J. (2017). The Emerging Roles of STING in Bacterial Infections. Trends Microbiol. 25, 906–918.

Martin, M., Hiroyasu, A., Guzman, R.M., Roberts, S.A., and Goodman, A.G. (2018). Analysis of Drosophila STING reveals an evolutionarily conserved antimicrobial function. Cell Rep 23, 3537–3550.e6.

McWhirter, S.M., Barbalat, R., Monroe, K.M., Fontana, M.F., Hyodo, M., Joncker, N.T., Ishii, K.J., Akira, S., Colonna, M., Chen, Z.J., et al. (2009). A host type I interferon response is induced by cytosolic sensing of the bacterial second messenger cyclic-di-GMP. J. Exp. Med. 206, 1899–1911.

Moghaddas, F., Zeng, P., Zhang, Y., Schützle, H., Brenner, S., Hofmann, S.R., Berner, R., Zhao, Y., Lu, B., Chen, X., et al. (2018). Autoinflammatory mutation in NLRC4 reveals a leucine-rich repeat (LRR)-LRR oligomerization interface. J. Allergy Clin. Immunol. 142, 1956–1967.e6.

Motwani, M., Pawaria, S., Bernier, J., Moses, S., Henry, K., Fang, T., Burkly, L., Marshak-Rothstein, A., and Fitzgerald, K.A. (2019). Hierarchy of clinical manifestations in SAVI N153S and V154M mouse models. Proc. Natl. Acad. Sci. USA 116, 7941–7950.

Ni, G., Konno, H., and Barber, G.N. (2017). Ubiquitination of STING at lysine 224 controls IRF3 activation. Sci. Immunol. 2, eaah7119.

Perry, A.K., Chow, E.K., Goodnough, J.B., Yeh, W.C., and Cheng, G. (2004). Differential requirement for TANK-binding kinase-1 in type I interferon responses to toll-like receptor activation and viral infection. J. Exp. Med. 199, 1651–1658.

Roberts, Z.J., Goutagny, N., Perera, P.Y., Kato, H., Kumar, H., Kawai, T., Akira, S., Savan, R., van Echo, D., Fitzgerald, K.A., et al. (2007). The chemotherapeutic agent DMXAA potently and specifically activates the TBK1-IRF-3 signaling axis. J. Exp. Med. 204, 1559–1569.

Rongvaux, A., Jackson, R., Harman, C.C., Li, T., West, A.P., de Zoete, M.R., Wu, Y., Yordy, B., Lakhani, S.A., Kuan, C.Y., et al. (2014). Apoptotic caspases

prevent the induction of type I interferons by mitochondrial DNA. Cell *159*, 1563–1577.

Saldanha, R.G., Balka, K.R., Davidson, S., Wainstein, B.K., Wong, M., Macintosh, R., Loo, C.K.C., Weber, M.A., Kamath, V., et al.; CIRCA; AADRY (2018). A Mutation Outside the Dimerization Domain Causing Atypical STING-Associated Vasculopathy With Onset in Infancy. Front. Immunol. *9*, 1535.

Sanchez, G.A.M., Reinhardt, A., Ramsey, S., Wittkowski, H., Hashkes, P.J., Berkun, Y., Schalm, S., Murias, S., Dare, J.A., Brown, D., et al. (2018). JAK1/2 inhibition with baricitinib in the treatment of autoinflammatory interferonopathies. J. Clin. Invest. *128*, 3041–3052.

Shimada, T., Kawai, T., Takeda, K., Matsumoto, M., Inoue, J., Tatsumi, Y., Kanamaru, A., and Akira, S. (1999). IKK-i, a novel lipopolysaccharide-inducible kinase that is related to IkappaB kinases. Int. Immunol. *11*, 1357–1362.

Sliter, D.A., Martinez, J., Hao, L., Chen, X., Sun, N., Fischer, T.D., Burman, J.L., Li, Y., Zhang, Z., Narendra, D.P., et al. (2018). Parkin and PINK1 mitigate STING-induced inflammation. Nature *561*, 258–262.

Smale, S.T. (2010). Selective transcription in response to an inflammatory stimulus. Cell *140*, 833–844.

Stempel, M., Chan, B., Juranić Lisnić, V., Krmpotić, A., Hartung, J., Paludan, S.R., Füllbrunn, N., Lemmermann, N.A., and Brinkmann, M.M. (2019). The herpesviral antagonist m152 reveals differential activation of STING-dependent IRF and NF-κB signaling and STING's dual role during MCMV infection. EMBO J. *38*, e100983.

Stetson, D.B., Ko, J.S., Heidmann, T., and Medzhitov, R. (2008). Trex1 prevents cell-intrinsic initiation of autoimmunity. Cell *134*, 587–598.

Sun, L., Wu, J., Du, F., Chen, X., and Chen, Z.J. (2013). Cyclic GMP-AMP synthase is a cytosolic DNA sensor that activates the type I interferon pathway. Science *339*, 786–791.

Tanaka, Y., and Chen, Z.J. (2012). STING specifies IRF3 phosphorylation by TBK1 in the cytosolic DNA signaling pathway. Sci. Signal. *5*, ra20.

Taniguchi, K., and Karin, M. (2018). NF-κB, inflammation, immunity and cancer: coming of age. Nat. Rev. Immunol. *18*, 309–324.

Tojima, Y., Fujimoto, A., Delhase, M., Chen, Y., Hatakeyama, S., Nakayama, K., Kaneko, Y., Nimura, Y., Motoyama, N., Ikeda, K., et al. (2000). NAK is an IkappaB kinase-activating kinase. Nature *404*, 778–782.

Warner, J.D., Irizarry-Caro, R.A., Bennion, B.G., Ai, T.L., Smith, A.M., Miner, C.A., Sakai, T., Gonugunta, V.K., Wu, J., Platt, D.J., et al. (2017). STING-associated vasculopathy develops independently of IRF3 in mice. J. Exp. Med. *214*, 3279–3292.

West, A.P., Khoury-Hanold, W., Staron, M., Tal, M.C., Pineda, C.M., Lang, S.M., Bestwick, M., Duguay, B.A., Raimundo, N., MacDuff, D.A., et al. (2015). Mitochondrial DNA stress primes the antiviral innate immune response. Nature *520*, 553–557.

White, M.J., McArthur, K., Metcalf, D., Lane, R.M., Cambier, J.C., Herold, M.J., van Delft, M.F., Bedoui, S., Lessene, G., Ritchie, M.E., et al. (2014). Apoptotic caspases suppress mtDNA-induced STING-mediated type I IFN production. Cell *159*, 1549–1562.

Woodward, J.J., Iavarone, A.T., and Portnoy, D.A. (2010). c-di-AMP secreted by intracellular Listeria monocytogenes activates a host type I interferon response. Science *328*, 1703–1705.

Xu, D., Jin, T., Zhu, H., Chen, H., Ofengeim, D., Zou, C., Mifflin, L., Pan, L., Amin, P., Li, W., et al. (2018). TBK1 suppresses RIPK1-driven apoptosis and inflammation during development and in aging. Cell *174*, 1477–1491.e19.

Zhang, X., Shi, H., Wu, J., Zhang, X., Sun, L., Chen, C., and Chen, Z.J. (2013). Cyclic GMP-AMP containing mixed phosphodiester linkages is an endogenous high-affinity ligand for STING. Mol. Cell *51*, 226–235.

Zhu, H.F., and Li, Y. (2018). Small-Molecule Targets in Tumor Immunotherapy. Nat. Prod. Bioprospect. *8*, 297–301.

Zitvogel, L., Galluzzi, L., Kepp, O., Smyth, M.J., and Kroemer, G. (2015). Type I interferons in anticancer immunity. Nat. Rev. Immunol. *15*, 405–414.

STAR★METHODS

KEY RESOURCES TABLE

REAGENT or RESOURCE	SOURCE	IDENTIFIER
Antibodies		
Rabbit monoclonal anti-NF-κB p65 (C22B4) antibody	Cell Signaling Technology	Cat# 4764; RRID:AB_823578
Rabbit monoclonal anti-NF-κB P-p65 Ser[536] (93H1) antibody	Cell Signaling Technology	Cat# 3033; RRID:AB_331284
Rabbit monoclonal anti-STING (D2P2F) antibody	Cell Signaling Technology	Cat# 13647; RRID:AB_2732796
Rabbit polyclonal anti-P-STING Ser[366] antibody (discontinued)	Cell Signaling Technology	Cat# 85735; RRID:AB_2801279
Rabbit monoclonal anti-P-STING Ser[366] (D7C3S) antibody	Cell Signaling Technology	Cat# 19781, RRID:AB_2737062
Rabbit monoclonal anti-P-STING Ser[365] (D8F4W) antibody	Cell Signaling Technology	Cat# 72971, RRID:AB_2799831
Rabbit polyclonal anti-TBK1 antibody	Cell Signaling Technology	Cat# 3013; RRID:AB_2199749
Rabbit monoclonal anti-P-TBK1 Ser[172] (D52C2) antibody	Cell Signaling Technology	Cat# 5483; RRID:AB_10693472
Rabbit monoclonal anti-IRF3 (D83B9) antibody	Cell Signaling Technology	Cat# 4302; RRID:AB_1904036
Rabbit monoclonal anti-P-IRF3 Ser[396] (4D4G) antibody	Cell Signaling Technology	Cat# 4947; RRID:AB_823547
Rabbit monoclonal anti-P-IKKε Ser[172] (D1B7) antibody	Cell Signaling Technology	Cat# 8766; RRID:AB_2737061
Rabbit monoclonal anti-IKKε (D61F9) antibody	Cell Signaling Technology	Cat# 3416; RRID:AB_1264180
Rabbit polyclonal anti-IκBα antibody	Cell Signaling Technology	Cat# 9242; RRID:AB_331623
Rabbit monoclonal anti-P-IKKα/β Ser[176/180] (16A6) antibody	Cell Signaling Technology	Cat# 2697; RRID:AB_2079382
Mouse monoclonal anti-TRAF6 (D-10) antibody	Santa Cruz Biotechnology	Cat# sc-8409; RRID:AB_628391
Mouse monoclonal anti-beta ACTIN, HRP (AC-15)	Abcam	Cat# Ab49900; RRID:AB_867494
Mouse 1gG2A monoclonal GFP (E36) antibody	Thermo Fisher Scientific	Cat# A-11120; RRID:AB_221568
Rat anti-mouse IFNβ (IFN-beta, IFNb, IFB, IFF, IFNB1, Fibroblast Interferon, MGC96956) antibody	USBiological Life Sciences	Cat# 138027
Rabbit polyclonal anti-Mouse IFNβ antibody	PBL Assay Science	Cat# 32400-1; RRID:AB_387872
Goat anti-Mouse IgG (H+L) Highly Cross-Adsorbed Secondary Antibody, HRP	Thermo Fisher Scientific	Cat# A16078; RRID:AB_2534751
Peroxidase-AffiniPure F(ab')2 Fragment Donkey Anti-Rabbit IgG (H+L) antibody	Jackson ImmunoResearch Labs	Cat# 711-036-152; RRID:AB_2340590
Peroxidase-AffiniPure Goat Anti-Rabbit IgG (H+L) antibody	Jackson ImmunoResearch Labs	Cat# 111-035-003; RRID:AB_2313567
Goat polyclonal anti-Rabbit IgG (H+L) Highly Cross-Adsorbed Secondary Antibody, Alexa-647	Thermo Fisher Scientific	Cat# A-21244; RRID:AB_2535812
Bacterial and Viral Strains		
HSV-1 (KOS strain)	Gabrielle Belz Laboratory	N/A
Listeria monocytogenes	Andrew Lew Laboratory	N/A
Biological Samples		
Human peripheral blood mononuclear cells (PBMCs)	Volunteer Blood Donor Registry (VBDR)	N/A
Chemicals, Peptides, and Recombinant Proteins		
Lipofectamine 2000 Transfection Reagent	Thermo Fisher Scientific	Cat# 11668030
Recombinant mouse IFNβ (carrier-free)	PBL Assay Science	Cat# 12401-1
DMXAA (5,6-Dimethylxanthenone-4-acetic acid)	InvivoGen	Cat# tlrl-dmx
2′3′-cGAMP - Cyclic [G(2′,5′)pA(3′,5′)p]	InvivoGen	Cat# tlrl-nacga23
2′3′-c-di-AM(PS)2 (Rp,Rp)	InvivoGen	Cat# tlrl-nacda2r

Continued

REAGENT or RESOURCE	SOURCE	IDENTIFIER
CpG DNA (1826)	InvivoGen	Cat# tlrl-1826
P3C (Pam3CysK4)	InvivoGen	Cat# tlrl-pms
Ultrapure LPS from *E. coli* 055:B5	InvivoGen	Cat# tlrl-pb5lps
Poly(I:C) high molecular weight	InvivoGen	Cat# tlrl-pic
Puromycin	InvivoGen	Cat# ant-pr-1
Hygromycin B Gold	InvivoGen	Cat# ant-hg-1
DMSO (Dimethyl sulfoxide)	Sigma-Aldrich	Cat# D2650
HT-DNA (DNA sodium salt from herring testes)	Sigma-Aldrich	Cat# D6898
Doxycycline hyclate	Sigma-Aldrich	Cat# D9891
MRT67307 (TBK1/IKKε kinase inhibitor)	Sigma-Aldrich	Cat# SML0702
TPCA-1 (IKKβ kinase inhibitor)	Sigma-Aldrich	Cat# T1452
5z-7-Oxozeaenol (TAK1 kinase inhibitor)	Sigma-Aldrich	Cat# O9890
WEHI-112 (TBK1/IKKε kinase inhibitor)	Walter and Eliza Hall Institute of Medical Research	(Louis et al., 2019)
Critical Commercial Assays		
NuPAGE 4-12% Bis-Tris Protein Gels, 1.5 mm, 10-well	Thermo Fisher Scientific	Cat# NP0335BOX
NuPAGE 4-12% Bis-Tris Protein Gels, 1.5 mm, 15-well	Thermo Fisher Scientific	Cat# NP0336BOX
NuPAGE 4-12% Bis-Tris Midi Protein Gels, 20-well	Thermo Fisher Scientific	Cat# WG1402A
NuPAGE MES SDS Running Buffer (20X)	Thermo Fisher Scientific	Cat# NP000202
Immobilon-P PVDF Membrane, 0.45 μm pore size, Hydrophobic PVDF	Merck Millipore	Cat# IPVH00005
cOmplete Protease Inhibitor Cocktail	Roche Biochemicals	Cat# 11836145001
Immobilon Forte Western HRP substrate	Merck Millipore	Cat# WBLUF0500
TNF alpha Mouse Uncoated ELISA Kit	Thermo Fisher Scientific	Cat# 88-7324-88
Nunc MaxiSorp flat-bottom ELISA plates	Thermo Fisher Scientific	Cat# 442404
μ–Slide 8 well	Ibidi	Cat# 80826
QuikChange Lightning Mutagenesis Kit	Agilent Technologies	Cat# 210513
Experimental Models: Cell Lines		
Human embryonic kidney (HEK) 293T cells	ATCC	CRL-3216
WT immortalized bone marrow-derived macrophages (iBMDMs)	Eicke Latz Laboratory	N/A
WT immortalized bone marrow-derived macrophages (iBMDMs) expressing Cas9-mCherry	This paper	N/A
WT immortalized bone marrow-derived macrophages (iBMDMs) expressing pTRIPZ empty vector (EV)	This paper	N/A
WT immortalized bone marrow-derived macrophages (iBMDMs) expressing WT hsSTING	This paper	N/A
WT immortalized bone marrow-derived macrophages (iBMDMs) expressing hsSTING R284S	This paper	N/A
TBK1[KO] immortalized bone marrow-derived macrophages (iBMDMs)	This paper	N/A
TBK1[KO] immortalized bone marrow-derived macrophages (iBMDMs) expressing pTRIPZ empty vector (EV)	This paper	N/A
TBK1[KO] immortalized bone marrow-derived macrophages (iBMDMs) expressing WT hsSTING	This paper	N/A
TBK1[KO] immortalized bone marrow-derived macrophages (iBMDMs) expressing hsSTING R284S	This paper	N/A
TRAF6[KO] immortalized bone marrow-derived macrophages (iBMDMs)	This paper	N/A

(Continued on next page)

Continued

REAGENT or RESOURCE	SOURCE	IDENTIFIER
IKKε^KO immortalized bone marrow-derived macrophages (iBMDMs)	This paper	N/A
TBK1^KO/IKKε^KO immortalized bone marrow-derived macrophages (iBMDMs)	This paper	N/A
Sting^−/− immortalized bone marrow-derived macrophages (iBMDMs)	This paper	N/A
WT THP-1 human monocytic cells	ATCC	TIB-202
WT THP-1 human monocytic cells expressing Cas9-mCherry	This paper	N/A
THP-1 TBK1^KO human monocytic cells	Ian Wicks Laboratory	(Louis et al., 2019)
THP-1 human monocytic cells expressing pTRIPZ empty vector (EV)	This paper	N/A
THP-1 human monocytic cells expressing WT human STING	This paper	N/A
THP-1 human monocytic cells expressing human STING R284S	This paper	N/A
Experimental Models: Organisms/Strains		
Tbk1^fl/fl (C56BL/6J-*Tbk1*^tm1.1 mrl) mice	Taconic	Model# 11131
Tbk1^fl/fl x *RosaCre*^+ (C56BL/6J) mice	This paper	N/A
C57BL/6J mice (for bone marrow-derived macrophages- BMDMs)	Jackson Laboratory	Cat# 000664
Sting^−/− mice (for bone marrow-derived macrophages- BMDMs)	Benjamin Kile Laboratory	N/A
Sting^+/+ mice (for bone marrow-derived macrophages- BMDMs)	Benjamin Kile Laboratory	N/A
Oligonucleotides		
Tbk1 targeting sgRNA	This paper	GAGGAGCCGTCCAATGCGTA
Ikbke targeting sgRNA	This paper	TGTCCAGCGACACACCTAAG
Traf6 targeting sgRNA	This paper	ATCCCGGGGATGTCGTCCAG
hsSTING ΔAgeI mutagenesis primer	This paper	CCCCAGCAGACAGGTGACCAT GCTGGC
hsSTING ΔAgeI PCR amplification forward primer	This paper	GCACCGGTATGCCCCACTCCAGCCTG
hsSTING ΔAgeI PCR amplification reverse primer	This paper	GCACGCGTTCAAGAGAAATCCGT GCGGAG
hsSTING R284S mutagenesis primer	This paper	GGCTTTAGCCGGGAGGATAGCCTTG AGCAGGCC
qPCR primer sequences		
Mouse *Hprt* forward	This paper	TGAAGTACTCATTATAGTCAAGGGCA
Mouse *Hprt* reverse	This paper	CTGGTGAAAAGGACCTCTCG
Mouse *Ifnb1* forward	This paper	CCAGCTCCAAGAAAGGACGA
Mouse *Ifnb1* reverse	This paper	TGGATGGCAAAGGCAGTGTA
Mouse *Ifna1* forward	This paper	CTACTGGCCAACCTGCTCTC
Mouse *Ifna1* reverse	This paper	CCTTCTTGATCTGCTGGGCA
Mouse *Ifna4* forward	This paper	CCTGTGTGATGCAGGAACC
Mouse *Ifna4* reverse	This paper	TCACCTCCCAGGCACAGA
Mouse *Il2b* forward	This paper	GGAAGCACGGCAGCAGAATA
Mouse *Il2b* reverse	This paper	ACTTGAGGGAGAAGTAGGAATGG
Mouse *Isg15* forward	This paper	TGTGAGAGCAAGCAGCCAGA
Mouse *Isg15* reverse	This paper	cccccagcatcttcaccttt
Mouse *Tnf* forward	This paper	CCAAATGGCCTCCCTCTCAT
Mouse *Tnf* reverse	This paper	TGGTGGTTTGCTACGACGTG
Mouse *Il1b* forward	This paper	TTGACGGACCCCAAAAGATG

Continued

REAGENT or RESOURCE	SOURCE	IDENTIFIER
Mouse *Il1b* reverse	This paper	CAGCTTCTCCACAGCCACAA
Mouse *Ccl4* forward	This paper	ACCTAACCCCGAGCAACACC
Mouse *Ccl4* reverse	This paper	GAGCCCATTGGTGCTGAGAA
Mouse *Il6* forward	This paper	CCAGAAACCGCTATGAAGTTCC
Mouse *Il6* reverse	This paper	CGGACTTGTGAAGTAGGGAAGG
Human *HPRT1* forward	This paper	TCAGGCAGTATAATCCAAAGATGGT
Human *HPRT1* reverse	This paper	AGTCTGGCTTATA TCCAACACTTCG
Human *ACTIN* forward	This paper	GCGAGAAGATGACCCAGATC
Human *ACTIN* reverse	This paper	CCAGTGGTACGGCCAGAGG
Human *IFNB1* forward	This paper	TGTCGCCTACTACCTGTTGTGC
Human *IFNB1* reverse	This paper	AACTGCAACCTTTCGAAGCC
Human *TNF* forward	This paper	TCTCTCAGCTCCACGCCATT
Human *TNF* reverse	This paper	CCCAGGCAGTCAGATCATCTTC
Recombinant DNA		
pEF-BOS-mCitrine-hsSTING	Veit Hornung Laboratory	N/A
pEF-BOS-mCitrine-hsSTING ΔAgeI	This paper	N/A
pTRIPZ Inducible Lentiviral Empty Vector (EV) Control	Dharmacon	Cat# RHS4750
pTRIPZ-hsSTING (ΔAgeI)	This paper	N/A
pTRIPZ-hsSTING (ΔAgeI) R284S	This paper	N/A
pMD2.G	Addgene	Plasmid #12259
psPAX2	Addgene	Plasmid# 12260
FUCas9mCherry	Addgene	Plasmid# 70182
pFgH1tUT-GFP	Addgene	Plasmid# 70183
pFgH1tUT-HygroR	This paper	N/A
pFgH1tUT-GFP *Tbk1* targeting sgRNA	This paper	N/A
pFgH1tUT- HygroR *Ikbke* targeting sgRNA	This paper	N/A
pFgH1tUT-GFP *Traf6* targeting sgRNA	This paper	N/A
Software and Algorithms		
FIJI	https://fiji.sc	RRID: SCR_002285
Image Lab	Bio-Rad Laboratories	RRID:SCR_014210
GraphPad Prism	https://www.graphpad.com/	RRID:SCR_002798
Adobe Illustrator	https://www.adobe.com/products/illustrator.html	RRID:SCR_010279

LEAD CONTACT AND MATERIALS AVAILABILITY

All unique/stable reagents generated in this study are available from the Lead Contact with a completed Materials Transfer Agreement. Further information and/or requests for resources and reagents should be directed to the Lead Contact, Dr Dominic De Nardo (dominic.denardo@monash.edu).

EXPERIMENTAL MODEL AND SUBJECT DETAILS

Animals

C57BL/6 wild-type, *Tbk1*^fl/fl^ (WT), *Tbk1*^fl/fl^ x *RosaCre* (TBK1 KO), *Sting*^+/+^ and *Sting*^−/−^ mice were housed under standard conditions at the Walter and Eliza Hall Institute Animal Facility. All procedures involving mice were approved by the Walter and Eliza Hall Institute Animal Ethics Committee. Male and female 8-week old *Tbk1*^fl/fl^ (WT) and *Tbk1*^fl/fl^ x *RosaCre* (TBK1 KO) mice received 3 mg tamoxifen by oral gavage per dosing for 4 consecutive days before intraperitoneal injection of either a DMSO control (Ctrl) or 500 μg (∼20 mg/kg) DMXAA diluted in 400 μL phosphate buffered saline (PBS) with 20% Captisol carrier solution. Mice were sacrificed 2h later for harvesting spleens.

Primary murine and human immune cells

Bone marrow cells were harvested from femurs and tibias of 6 to 8-week old male or female mice and cultured with complete Dulbecco's Modified Eagle Medium (DMEM, Thermo Scientific) [DMEM with 1% (w/v,) D-glucose, 0.11% (w/v) sodium pyruvate, 0.1% (w/v) streptomycin, 100u/mL penicillin and 10% fetal bovine serum (FBS) (Sigma-Aldrich)] supplemented with 20% L929 conditioned media for six days at 37°C in humidified atmosphere with 5% CO_2 to generate primary bone marrow-derived macrophages (BMDMs). Human peripheral blood mononuclear cells (PBMCs) were isolated from whole blood over a Ficoll density gradient (GE Healthcare) with the approval of the Walter and Eliza Hall Institute Human Research Ethics Committee. Following several washes with phosphate buffered saline (PBS) PBMCs were cultured in complete Roswell Park Memorial Institute media 1640 (RPMI-1640) [1% (w/v) RPMI-1640, 0.2% (w/v) $NaHCO_3$, 0.011% (w/v) $C_3H_3NaO_3$, 0.1% (w/v) streptomycin, 100u/mL penicillin, supplemented with 10% FBS] at 37°C in humidified atmosphere with 5% CO_2.

Immortalized cell lines

Human Embryonic Kidney 293T (HEK293T) cells and iBMDMs were cultured in complete DMEM at 37°C in 5% CO_2 humidified atmosphere. THP-1 human monocyte-like cells were maintained in complete RPMI at 37°C in humidified atmosphere with 5% CO_2.

Sting$^{-/-}$ immortalized BMDMs (iBMDMs)

Sting$^{-/-}$ iBMDMs were generated as described (De Nardo et al., 2018b). Bone marrow cells from Sting$^{-/-}$ mice were harvested from the femurs of an 8-week old male mouse and cultured with complete DMEM supplemented with 20% L929 conditioned media for two days. Cells were then subjected to J2 recombinant retrovirus (50%) in DMEM supplemented with 20% L929 conditioned media for 24 h, before further culture in DMEM with 20% L929 conditioned media for 4 days to generate BMDMs. Cells were subsequently cultured for ~3 months with gradual reductions of L929 conditioned media until they were able to survive and proliferate in the absence of any L929. At this point cells were considered immortalized and phenotypically and functionally tested in comparison with primary BMDMs.

Gene knockout cells via CRISPR/Cas9

TBK1^{KO}, IKKε^{KO}, TBK1^{KO}/IKKε^{KO} and TRAF6^{KO} iBMDMs were generated by CRISPR/Cas9 gene editing as previously described (Baker and Masters, 2018). Third generation lentiviral transduction was used to generate WT iBMDMs expressing Cas9 fused to mCherry (using the FUCas9mCherry plasmid), which were subsequently enriched by FACS sorting. Doxycycline-inducible sgRNA plasmids (using pFgH1tUT plamids) targeting specific genes of interest were then introduced into iBMDMs expressing Cas9-mCherry via third generation lentiviral transduction (described below). Cells expressing sgRNA plasmids were then enriched by either FACS or antibiotic selection. Gene disruption was confirmed by immunoblot analysis of target proteins and functional analysis. The sgRNA targeting sequences used are provided in the Key Resources Table.

METHOD DETAILS

Generation of lentiviral plasmids

The second-generation pTRIPZ-hsSTING lentiviral plasmid expressing a doxycycline-inducible human STING, was generated by amplifying STING ΔAgeI cDNA from a template plasmid (pEF-BOS-mCitrine-hsSTING ΔAgeI) before the resultant PCR product was digested with AgeI and MluI and cloned in-frame into the corresponding sites of pTRIPZ. The pTRIPZ-hsSTING (ΔAgeI) plasmid was then used to generate pTRIPZ-hSTING R284S (ΔAgeI) using the QuikChange Lightning Mutagenesis Kit (Agilent Technologies). Third-generation sgRNA plasmids were generated by annealing specific sgRNA oligo sequences before ligation into BsmBI sites of pFgH1tUT (GFP or HygroR). Plasmids were subsequently subjected to sanger sequencing (Australian Genome Research Facility [AGRF] or Monash Micromon). All primer sequences used are listed in the Key Resources Table.

Lentiviral transduction

Lentiviral transduction of THP-1 human monocyte-like cells or iBMDMs was performed similarly to published viral transduction protocols (Cardona Gloria et al., 2018; Moghaddas et al., 2018). Third-generation lentivirus was generated by transient transfection of HEK293T cells with lentiviral plasmids (FUCas9mCherry, pFgH1tUT), pMDL (packaging), RSV-REV (packaging) and VSVg (envelope) plasmids complexed into liposomes using Lipofectamine 2000 (Thermo Scientific) diluted in OptimMEM (Thermo Scientific). Second-generation lentivirus was generated via transient transfection of HEK293T cells with lentiviral pTRIPZ, pPAX2 (packaging) and pMD2.G (envelope) plasmids complexed into liposomes using Lipofectamine 2000 (Thermo Scientific) diluted in OptimMEM (Thermo Scientific). Third- and second-generation lentiviruses were harvested 48 h later, filtered through 0.45 μm filters and used to infect THP-1 or iBMDMs target cell lines. Cells were subsequently enriched for lentiviral plasmid expression via antibiotic selection or FACS sorting.

Preparation of whole-cell lysates (WCLs)

For immunoblot assays, ~1-1.5 × 10^6 THP-1 monocytes, iBMDMs or primary BMDMs were lysed on ice with 150 μl of 1 x Radio-immune precipitation assay (RIPA) buffer [20 mM Tris-HCl pH 7.4, 150 mM NaCl, 1 mM EDTA, 1% Triton X-100, 10% glycerol,

0.1% SDS and 0.5% deoxycholate, 5mM NaF, 10mM NaPP$_i$, 1mM Na$_3$VO$_4$] supplemented with 1mM phenylmethylsulfonyl fluoride (PMSF) and 1 x cOmplete protease inhibitors (Roche Biochemicals). WCLs were clarified by centrifugation at 17,000 x g for 1 min through Pierce centrifuge columns (Thermo Scientific) before 60 μL was diluted with 20 μL 4x reducing SDS-PAGE sample loading buffer [1.25% SDS, 12.5% glycerol, 62.5 mM Tris-HCl pH 6.8, 0.005% bromophenol blue, 50 mM dithiothreitol] and heated to 95°C for 10 min.

Immunoblotting

Between 20-35 μl of prepared WCL samples were run on NuPAGE 4%–12% Bis-Tris Protein Gels (Thermo Scientific) with MES or MOPS running buffer (Thermo Scientific). Following activation of Immobilon-P polyvinyl difluoride (PVDF) membrane (Millipore Merk) in methanol, proteins were transferred to membranes using the Trans-Blot Turbo System (BioRad). Membranes were then blocked using 5% skim milk powder in Tris buffered saline (TBS) + 0.1% Tween 20 (TBST) at room temperature (RT) for 1 h before incubation overnight in primary antibodies at 4°C. Membranes were then washed 3x in TBST (10-20 min per wash) and incubated with appropriate secondary antibodies for 1-2 h at RT before membranes were again washed 3x in TBST. Chemiluminescence was detected by subjecting membranes to Immobilon Forte Western HRP substrate (Millipore Merk) before imaging using the ChemiDoc Touch or ChemiDoc XRS+ Imaging Systems (BioRad). Images were acquired and converted to tagged image format file (TIFF) using Image Lab software (BioRad). When required protein was removed from membranes using a mild stripping buffer [1.5% glycine, 1% SDS, 0.01% Tween 20, pH 2.2] before 3x washes in TBST and re-probing with primary antibodies. Primary and secondary antibodies used for immunoblot used are listed in the Key Resources Table.

Quantitative real time-PCR

RNA was purified from ~1 × 10^6 THP-1 monocytes or iBMDMs, 1.2 × 10^6 BMDMs or 2.5 × 10^6 PBMCs using either the EZ-10 DNAaway RNA Miniprep Kit (Bio Basic), or > 30 mg of splenic tissue using the ISOLATE II RNA mini kit (Bioline) according to the manufacturer's instructions. cDNA was generated using SuperScript III Reverse Transcriptase (Thermo Scientific). Quantitative real-time PCR (qPCR) was performed using Maxima SYBR Green/ROX qPCR Master Mix (Thermo Scientific) on a Viia 7 real-time PCR system (Thermo Scientific). Expression levels were normalized to human (*HPRT1* or *ACTIN*) or murine (*Hprt*) housekeeping genes. Specific primer sequences used are listed in the Key Resources Table.

Enzyme-Linked Immunosorbent Assay (ELISA)

Cell supernatant was assayed for murine TNF using eBioscence kit (Thermo Scientific) according to the manufacturer's protocol. Murine IFNβ was measured using a custom-made protocol as previously reported (Roberts et al., 2007). The monoclonal rat anti-mouse IFNβ (USBiological Life Sciences; 138027) was used as a coating antibody, while the polyclonal rabbit anti-mouse IFNβ (PBL Assay Science; 32400-1) was used for detection. Recombinant mouse IFNβ (carrier-free) (PBL Assay Science; 12401-1) was used to generate a standard curve, peroxidase-conjugated AffiniPure F(ab')$_2$ fragment donkey anti-rabbit IgG (H+L) (Jackson Immuno Research; 711-036-152) was used for chemiluminescence, and PBS with 1% bovine serum albumin (BSA) was used as the assay diluent.

Immunofluorescence

Immunofluorescence of NF-κB p65 and IRF3 nuclear translocation was performed as previously described (De Nardo et al., 2018a). 1-2 x10^5 BMDMs were plated in 8-well μ-slides (Ibidi). Following experimentation cells were fixed with 4% paraformaldehyde for 10 min before blocking and permeabilizing cells (Block/Perm buffer: PBS, 10% (v/v) FCS, 0.5% Triton X-100) for 1 hr at room temperature. Cell were then stained with anti-NF-κB p65 primary antibody (Cell Signaling Technology: clone C22B4, 4764, 1:100) or anti-IRF3 (Cell Signaling Technology; clone D83B9, 4302, 1:100) overnight at 4°C. The following day cells were stained with a secondary goat anti-rabbit Alexa-647 antibody (Thermo Scientific; A-21244, 1:1000) before nuclear staining with DAPI (1 μM) for 5-10 min at room temperature. Between steps cells were washed 3 times with Block/Perm buffer or PBS. Imaging was performed using a Zeiss LSM 780 confocal microscope; 3x3 tile scans were taken for each experimental condition using a 63x oil objective with Immersol 518 F (Zeiss) and acquired with ZEN 2012 version 8.1 software (Zeiss). Image channels were merged before conversion to TIFF using FIJI software. Quantification of nuclear staining was performed using FIJI software by identifying DAPI positive nuclei and measuring the mean fluorescent intensity of the Alexa-647 channel within each nucleus.

QUANTIFICATION AND STATISTICAL ANALYSIS

Analyses were performed with Prism (GraphPad Software) and data are typically presented as the mean +SEM, where a p value < 0.05 was considered significant as determined by paired or unpaired two-tailed Student t tests or a Mann Whitney test as indicated in the specific figure legends.

DATA AND CODE AVAILABILITY

No datasets or code were generated in this study.